The LRRC8A:C Heteromeric Channel Is a cGAMP Transporter and the Dominant cGAMP Importer in Human Vasculature Cells

Lauren J. Lahey[1,2], Xianlan Wen[3], Rachel E. Mardjuki[2,4], Volker Böhnert[2,5], Christopher Ritchie[2,5], Jacqueline A. Carozza[2,4], Gaelen T. Hess[2,6], Merritt Maduke[3], Michael C. Bassik[2,6], and Lingyin Li[2,5,7,*]

[1]Biophysics Program, [2]Stanford ChEM-H, [3]Department of Molecular and Cellular Physiology, [4]Department of Chemistry, [5]Department of Biochemistry, [6]Department of Genetics, Stanford University School of Medicine, Stanford, CA 94305 USA.

[7]Lead Contact

*Correspondence: lingyinl@stanford.edu

SUMMARY

Extracellular 2'3'-cyclic-GMP-AMP (cGAMP) is an immunotransmitter secreted by cancer cells and taken up by host cells to activate the anti-cancer STING pathway. No cGAMP exporter has been identified, and SLC19A1, a recently identified cGAMP importer, does not account for the import activity in most cell types. Here, we identify the LRRC8A:C heteromeric channel, a volume-regulated anion channel (VRAC), as a cGAMP transporter. This channel mediates cGAMP import or export depending on the cGAMP chemical gradient. cGAMP influences anion influx through VRAC, indicating it is likely a direct substrate of the channel. Activation or inhibition of the channel modulates cGAMP transport. The LRRC8A:C channel also transports other 2'3'-cyclic dinucleotides, including the investigational new cancer therapeutic ADU-S100. Furthermore, we demonstrate that the LRRC8A-containing channel is the dominant cGAMP importer in primary human vasculature cells, indicating that modulation of this channel represents a promising strategy to boost therapeutic STING signaling in tumor vasculature.

INTRODUCTION

A potent and versatile immune signaling molecule, 2'3'-cyclic-GMP-AMP (cGAMP) is a second messenger that relays detection of pathogen- or damage-associated threats to the activation of innate immunity. cGAMP is synthesized in the cytosol of metazoan cells when cytosolic dsDNA is recognized by cyclic-AMP-GMP synthase (cGAS)[1–5]. Cytosolic dsDNA is a conserved danger signal that can arise from diverse threats to a cell: infection by dsDNA viruses[6], retroviruses[7], or bacteria[8,9], but also damage[10–12],

cancerous state[13,14], or senescence[15–17]. Once synthesized, cGAMP activates its receptor, Stimulator of Interferon Genes (STING)[2–4], to trigger activation of TBK1 and IRF3 signaling[18–20]. The resulting production of type I interferons and other cytokines then induces powerful inflammatory and defense responses[21]. However, aberrant activation of this pathway, such as from DNAse deficiencies[7,22] or mitochondrial damage[12], can lead to deleterious effects such as autoimmune symptoms[23] and neuroinflammation in Parkinson's disease[24]. In order to understand the crucial roles cGAS-STING signaling in homeostasis and disease, it is imperative to determine how nature regulates the potent central messenger of the system, cGAMP, including its trafficking and transport.

We now know that cGAMP is not only a cell-intrinsic activator of STING, but also a paracrine signal. During viral infection, cGAMP crosses the cell membrane via gap junctions to activate immediately adjacent cells[25], and also gets packaged in viral particles and delivered to other cells in the vicinity[26,27]. Recently, we reported that cGAMP can be directly exported into the extracellular space in a soluble, non-membrane bound form[28]. Once outside the cell, cGAMP plays a pivotal role in anti-cancer immunity. Cytosolic dsDNA is a prominent characteristic of cancers with high chromosomal instability[10,13,14], and we demonstrated that cancer cells basally produce and export cGAMP. This secreted, extracellular cGAMP leads to an increase in innate immune cells within the tumor microenvironment and contributes to the curative effect of ionizing radiation in a STING-dependent manner[28].

Despite this newly discovered extracellular role of cGAMP in eliciting antitumoral immune responses, there remains a large gap in knowledge as to how cellular transport of cGAMP is achieved. cGAMP, a negatively charged molecule, must rely on facilitated mechanisms to cross the plasma membrane. While we and others identified the reduced folate carrier SLC19A1 as the first importer of cGAMP[29,30], our studies indicated the presence of additional cGAMP transport mechanisms. We were unable to identify a primary human cell type that uses SLC19A1 as its dominant cGAMP import mechanism[29]. Moreover, the identity of the cGAMP exporter(s) in cancer cells is currently unknown. Discovery of additional cGAMP transport mechanisms is therefore imperative to understand the extent, selectivity, and regulation of extracellular cGAMP signaling in homeostasis and disease.

Furthermore, identification of cGAMP import routes has important implications for development of STING-targeting therapeutics. We and others have created cGAMP analogs as potential anti-cancer agents, including 2'3'-cG^{S}A^{S}MP[31] and 2'3'-CDA^{S} (also known as ADU-S100)[32] that use stable phosphorothioate linkages in place of hydrolysable phosphodiester linkages. When intratumorally injected, these compounds exert curative effects in multiple mouse tumor models[32] and cGAMP analogs have now entered phase I and II clinical trials (ClinicalTrials.gov: NCT02675439, NCT03172936, and NCT03937141). Within the tumor microenvironment, injected STING agonists are sensed by stromal cells, tumor vasculature, and hematopoietic cells to elicit antitumoral immune responses[32–34]. However, activation of STING signaling in T cells may be therapeutically detrimental as is it can lead to antiproliferative effects and/or death of

these cells[9,35–37]. T cell-specific toxicity may explain the bell-shaped dose-response curve of 2'3'-CDA^S in which the highest drug concentrations impaired generation of the tumor-specific T cell responses necessary for durable anti-cancer immunity[38]. Elucidating how each cell type imports cGAMP analogs will inform whether therapeutic design and delivery can be improved to selectively target desired cell types.

Here, through a whole-genome CRISPR screen in SLC19A1 knockout cells, we identified a second direct transporter of cGAMP to be the LRRC8A:C heteromeric channel. LRRC8A was recently identified as an essential component of the long sought-after volume-regulated anion (VRAC) channel[39,40]. Beyond VRAC's role in regulating cell-intrinsic physiology, LRRC8A-containing channels are now being discovered to mediate cell-cell communication via transport of signaling molecules[41], for example the neurotransmitter glutamate[42]. In establishing a connection between the burgeoning fields of cGAMP signaling in innate immunity and LRRC8A channel function, this prompts new avenues of research into the biological relationship between these processes and their ability to be therapeutically regulated.

RESULTS

A Genome-Wide CRISPR Screen Identifies LRRC8A as a Positive Regulator of Extracellular cGAMP-Mediated STING Pathway Activation

We previously identified SLC19A1 as the first cGAMP importer by performing a whole-genome CRISPR knockout screen in the U937 cell line[29]. While SLC19A1 was the dominant importer in U937 cells, the existence of additional cGAMP import pathways

was evident from the residual signaling observed in *SLC19A1*$^{-/-}$ cells[29]: extracellular cGAMP treatment still led to activation of STING and downstream phosphorylation of STING, the kinase TBK1, and the transcription factor IRF3, ultimately resulting in cytokine production and cell death (Figure 1A). To identify these SLC19A1-independent import mechanisms, we performed a whole-genome CRISPR knockout screen[43] in U937 Cas9-*SLC19A1*$^{-/-}$ cells. We determined that ~30 μM extracellular cGAMP was a 50% lethal dose (LD_{50}) in U937 Cas9-*SLC19A1*$^{-/-}$ cell at 48 hours (Figure S1C), suggesting that our previous live/dead screen approach could again be employed. We treated the library daily for 12 days with cGAMP, increasing from 15 μM to 30 μM, while passaging untreated cells in parallel as controls (Figure 1B). In principle, cells harboring an sgRNA that knocks out a positive regulator of the extracellular cGAMP-STING pathway, including a cGAMP importer, should be enriched for via resistance to cGAMP-mediated cell death. Conversely, cells should be depleted if they harbor sgRNAs targeting negative regulators of the pathway. At the end of the selection, we isolated genomic DNA from each condition and sequenced the encoded sgRNAs. We then analyzed fold changes of sgRNA sequences in cGAMP treated cells versus controls using the Cas9 high-Throughput maximum Likelihood Estimator (casTLE) statistical framework to calculate a casTLE score and effect for each gene[44]. Key STING pathway components, *TMEM173* (STING), *TBK1*, and *IRF3*, were reproducibly identified with high confidence scores (Figure 1C) and large effect sizes (Figure 1D), validating this screening approach. Interestingly, *LRRC8A* clustered near known STING pathway members (Figure 1C – 1D).

LRRC8A and LRRC8 Paralogs Differentially Facilitate cGAMP Import

LRRC8A was recently identified as an essential component of the volume-regulated anion channel (VRAC) that resides on the plasma membrane[39,40]. Upon cell swelling or sensing of various stimuli, opening of VRAC leads to outward flow of chloride ions, organic osmolytes, and water to facilitate regulated volume decrease[41,45,46]. In order to form channels with functional VRAC activity in cells, LRRC8A must associate with one or more paralogous proteins, LRRC8B–E[40]. These channels are reported to be heteromeric hexamers in which subunit stoichiometry may be variable[47,48]. Depending on the paralog(s) in complex with LRRC8A, the channel exhibits different properties[49] and can transport different substrates. While complexes containing LRRC8B–E mediate inorganic anion flux, LRRC8A:C, LRRC8A:D, and LRRC8A:E complexes transport larger anionic substrates such as glutamate and aspartate[47,48,50,51]. LRRC8A:C and LRRC8A:E channels have been reported to transport ATP[47]. Distinct characteristics of LRRC8D-containing channels have been reported, including mediating efflux of uncharged cellular osmolytes[51] and import of the drugs blasticidin, cisplatin, and carboplatin[50,52]. It is therefore plausible that LRRC8A forms heteromeric channels with other LRRC8 paralogs to import extracellular cGAMP.

In our screen, *LRRC8C* and *LRRC8E* had moderate and weak positive effect sizes, respectively, and *LRRC8D* had a negative effect size (Figure 1C). To investigate the role of all LRRC8 paralogs in extracellular cGAMP signaling, we individually knocked out each gene in U937 *SLC19A1*$^{-/-}$ cells using multiple gene-specific sgRNAs. We also used a non-targeting scrambled sgRNA to serve as a negative control. We then isolated

and validated single cell clones, treated them with extracellular cGAMP, and measured phosphorylation of IRF3 (p-IRF3) to assess STING pathway activation (Figure S2). LRRC8A knockout clones exhibited a ~40% reduction in p-IRF3 relative to total IRF3 as compared to scramble controls, while LRRC8C knockout clones exhibited a ~30% reduction (Figure 2A). In contrast, a ~40% increase in p-IRF3 signaling was observed in LRRC8D knockout clones. Negligible differences were observed in LRRC8B and LRRC8E knockouts (average decreases of 5% and 8%, respectively), consistent with LRRC8B not playing a role in transport of large anions[48,51] and LRRC8E expression being restricted[41]. Together, these data validate the effects observed in the whole-genome screen that LRRC8 paralogs play differential regulatory roles in extracellular cGAMP signaling.

We then tested whether LRRC8 paralogs affect the response to cGAMP at the level of import or by altering downstream STING pathway signaling. When cGAMP was electroporated into the cells, bypassing the need for specific importers, *LRRC8A*$^{-/-}$ through *LRRC8E*$^{-/-}$ clones no longer exhibited differential p-IRF3 signaling compared to scramble controls (Figure 2B). Our data support a model in which LRRC8A, likely in complex with LRRC8C, facilitates transport of extracellular cGAMP across the plasma membrane. Our data also demonstrate that LRRC8D negatively affects this process, possibly by sequestering LRRC8A into heteromeric complexes that are not functional for mediating cGAMP import.

LRRC8A-Containing VRAC Channels Directly Transport cGAMP

We next sought to determine whether cGAMP is directly transported by LRRC8A channels. Alternatively, VRAC activation could alter membrane potential to influence cGAMP transport through another route not revealed by our CRISPR screen. Much of the work dissecting VRAC function has been performed in HEK293 cells[45,53], which we previously determined respond to extracellular cGAMP in an SLC19A1-independent manner[29]. Following the generation of LRRC8 knockout pools and validation of gene editing (Figure S3A), we tested whether these channels facilitate cGAMP import in HEK293 cells. Using the most upstream reporter of cGAMP import, phosphorylation of STING (p-STING) following cGAMP binding, we observed that HEK293 LRRC8A knockout pools exhibited a ~20% decrease in cellular response to extracellular cGAMP compared to controls (Figure 3A). Conversely, LRRC8D knockout pools exhibited a ~30% increase in extracellular cGAMP response. These results suggest that LRRC8 channels also facilitate import of cGAMP in HEK293 cells, although they do not account for the dominant mechanism. Consistent with our observations in U937 cells, LRRC8 paralogs differentially affect the cGAMP import process in HEK293 cells.

If LRRC8A channels directly transport cGAMP, we should be able to observe cGAMP efflux by i) inverting the cGAMP gradient to a high intracellular concentration and ii) triggering VRAC opening. Activation of VRAC is commonly experimentally achieved by application of hypotonic extracellular buffer[39,40]. It is worth noting that VRAC-mediated export of another nucleotide, ATP, has been demonstrated upon channel opening[47,54,55]. We stimulated intracellular cGAMP synthesis in HEK293 scramble control, LRRC8A, or LRRC8D knockout pools by transfecting cells with a cGAS expression plasmid.

Degradation of cGAMP by its hydrolase, ENPP1, was inhibited using the small molecule inhibitor STF-1084[28]. After 24 hours, we harvested the media from each condition and treated cells with a hypotonic buffer for 20 minutes to stimulate channel opening. We then measured cGAMP in these extracellular solutions. We detected cGAMP secreted into the media at levels similar to those previously reported, but observed no notable differences between scramble, LRRC8A, and LRRC8D knockout pools (64, 75, and 71.4 nM, respectively), suggesting that LRRC8A channels are not major exporters of cGAMP in HEK293 cells under resting conditions (Figure 3B). In contrast, we detected markedly higher cGAMP export from control (72 nM) and LRRC8D knockout cells (93 nM) compared to LRRC8A knockout cells (16 nM) upon hypotonic treatment (Figure 3B). These data suggest that LRRC8A-containing channels, when opened, mediate cGAMP export.

We next tested whether cGAMP directly interacts with LRRC8A channels. Previous work using electrophysiology has shown that extracellular ATP inhibits Cl^- influx via VRAC and that this inhibition is the result of direct pore block[56–58]. We tested whether extracellular cGAMP also blocks Cl^- influx through VRAC. Whole-cell patch clamp analysis of HEK293 cells revealed that the characteristic, hypotonic solution-induced VRAC current measured at positive membrane potential is inhibited by introduction of cGAMP in the bath solution (Figure 3C, 3D, and Figure S3B). Similar to inhibition by ATP (Figure S3C), inhibition by cGAMP is rapid and reversible, providing strong support for the conclusion that cGAMP directly interacts with the LRRC8A-containing VRAC channel. The observed inhibition is also consistent with cGAMP being directly

transported by the LRRC8A-containing channels: larger substrates that are transported slowly generally act as inhibitors ("permeating blockers") of fast traveling smaller ions through channels[59]; ATP was previously shown to be a such a permeating blocker of Cl^- influx through VRAC[55]. Therefore, it is likely that cGAMP, like ATP, is permeating through the LRRC8A channel.

The LRRC8A:C Channel Is the Dominant cGAMP Importer in Microvasculature Cells

Our LRRC8 subunit analysis performed in U937 and HEK293 cells predicts that cell types expressing high levels of LRRC8A and LRRC8C and low levels of LRRC8D should import cGAMP effectively. We evaluated RNA expression profiles of different cell types in The Human Protein Atlas (proteinatlas.org) and identified that several vasculature cell lineages fit such a profile (Figure S4A). TIME cells, an immortalized human microvascular endothelial cell (HMVEC) line, express *LRRC8A* and *LRRC8C* transcripts at 15.2-fold and 1.6-fold higher levels, respectively, than U937 cells while expressing *LRRC8D* transcripts at a 4.3-fold lower level. Indeed, TIME cells responded to extracellular cGAMP with an EC_{50} of ~24 μM (Figure S4B), which is more sensitive than most cell lines we have evaluated to date, including U937 cells with an EC_{50} of 270 μM[29]. To determine if cGAMP import depends on LRRC8 complexes in these cells, we knocked out LRRC8A–E using CRISPR, as well as the first identified importer, SLC19A1 (Figure S4C). LRRC8A or LRRC8C knockout in TIME cells resulted in loss of the majority of response to extracellular cGAMP, as measured by phosphorylation of all key pathway components: p-STING, p-TBK1, and p-IRF3 (Figure 4A). LRRC8D

knockout cells trended towards a modestly increased p-STING response, the amplitude of which is lower than in U937 or HEK293 cells, likely reflective of lower *LRRC8D* expression in TIME cells (Figure S4A). No significant effect was observed upon SLC19A1 knockout, confirming that this importer is not broadly used and that cGAMP import mechanisms are cell-type specific. Bypassing the need for specific importers using lipid-based transfection of cGAMP into cells resulted in similar responses across scramble, LRRC8A, LRRC8C and LRRC8D knockout pools (Figure 4B), again supporting a role for LRRC8A and LRRC8C in transport of cGAMP across the plasma membrane. Knockout of both LRRC8A and LRRC8C did not have an additive effect compared to single knockouts (Figure 4C). Given the known requirement of LRRC8A and at least one other subunit for cellular VRAC function[40,49], our results are consistent with LRRC8A and LRRC8C forming heterometric complexes to import cGAMP.

To demonstrate that the effect of the CRISPR knockout is due to loss of LRRC8A and LRRC8C proteins, but not off-target effects of the CRISPR procedures, we next tested whether rescued expression of each protein restored signaling in the corresponding knockout TIME cells. Standard expression by transient transfection would result in plasmid DNA activating cGAS, production of cGAMP, and high basal STING pathway activation. Therefore, we generated stable cell lines in which LRRC8A-Flag and LRRC8C-Flag expression is driven from a tetracycline-inducible promoter. Unfortunately, we were not able to overexpress LRRC8D to probe its inhibitory role in these cells as its expression was consistently low or undetectable. Regardless, we observed concentration-dependent increases in extracellular cGAMP response when

we restored LRRC8A and LRRC8C protein expression (Figure 4D). As revealed by recent cryo-electron microscopy structures of LRRC8A homomeric complexes[58,60,61], the narrowest region of the LRRC8A channel is gated by an arginine residue (R103), creating a strong positive charge potential at the extracellular pore. LRRC8C has a leucine residue at the corresponding position. The phosphodiester ring of cGAMP is double-negatively charged, therefore we predicted that R103 contributed by the LRRC8A subunit is crucial for cGAMP recognition. To test this hypothesis, we overexpressed the LRRC8A-R103L mutant in LRRC8A knockout cells and observed that it did not rescue cellular response to extracellular cGAMP (Figure 4D). This result supports a role for the pore-gating residue R103 in cGAMP recognition in a manner that is consistent with charge-charge interactions regulating channel access. Collectively, these data demonstrate that the LRRC8A:C complex functions as the dominant cGAMP importer in TIME cells.

cGAMP Import by the LRRC8A:C Channel Can Be Potentiated by Sphingosine-1-Phosphate and Inhibited by DCPIB

After establishing the dominance of the LRRC8A:C cGAMP import pathway observed in TIME cells, we next wanted to identify tools to regulate its function. VRAC has been shown to be activated downstream of sphingosine-1-phosphate (S1P) signaling to one of its G protein-coupled receptors, S1PR1[62]. In addition, endothelial cells are exposed to high S1P levels in the blood under physiological conditions (estimated 1 μM total), and also produce S1P themselves[63]. TIME cells are cultured with 5% fetal bovine serum, which we estimate to contain a maximum of 50 nM S1P. We hypothesized that

increasing S1P closer to physiological levels would further increase cGAMP uptake by TIME cells *in vitro*. Additionally, we sought to determine the effect of DCPIB (Figure 5A), a known small molecule VRAC inhibitor[39,64], on the response to extracellular cGAMP. The recently solved structure of a LRRC8A homomeric complex with DCPIB revealed that the inhibitor binds within the narrow pore formed by R103, effectively acting like a "cork in the bottle"[65]. Since cGAMP uptake also required R103, we anticipated that DCPIB should inhibit cGAMP import. Indeed, S1P increased extracellular cGAMP signaling by 2- to 3-fold in a dose- and LRRC8A-dependent manner (Figure 5B), but did not lead to STING signaling in the absence of cGAMP (Figure S5). Conversely, DCPIB significantly inhibited all LRRC8A-dependent extracellular cGAMP signaling under both basal and S1P-stimulated conditions. Together, our results suggest that LRRC8A:C channel uptake of cGAMP into TIME cells is potentiated by physiological concentrations of S1P. In addition, DCPIB can be used as a tool to specifically study LRRC8A-dependent cGAMP import.

The LRRC8A:C Channel Imports Other 2'3'-Cyclic Dinucleotides

We next evaluated the specificity of LRRC8A complexes for import against a broad panel of natural and synthetic cyclic dinucleotides (CDNs) (Figure 6A). Synthetic non-hydrolyzable phosphorothioate cGAMP analogs 2'3'-cG^{S}A^{S}MP and 2'3'-CDA^{S} have been designed as potent STING agonists for innate immunotherapy[31,32], and 2'3'-CDA^{S} is undergoing evaluation in clinical trials for treatment of metastatic cancers (ClinicalTrials.gov: NCT02675439, NCT03172936, and NCT03937141). Additionally, bacteria produce CDN second messengers with a different 3'3'-phosphodiester linkage

between nucleotides. Bacterial CDNs include 3'3'-cyclic-GMP-AMP (3'3'-cGAMP), 3'3'-cyclic-di-GMP (3'3'-CDG), and 3'3'-cyclic-di-AMP (3'3'-CDA)[4,66,67], which can trigger host STING signaling upon infection[67–69]. We observed that LRRC8A channels account for the majority of cGAMP, 2'3'-cG^{S}A^{S}MP, and 2'3'-CDA^{S} import in TIME cells, while playing a minor role in 2'3'-CDA import and negligible role in the import of all 3'3'-CDNs (Figure 6B).

LRRC8A-Containing Channels Are the Dominant cGAMP Importer in Primary Human Endothelial Cells, but Not in PBMCs

Extracellular cGAMP is known to play pivotal roles in tumor detection[28] and both tumor vasculature and infiltrating immune cells have been implicated in STING-dependent anti-cancer responses[32–34,38]. Therefore, we sought to determine the contribution of LRRC8A channels to cGAMP uptake across physiologically important responder cell types. These results would inform whether LRRC8A-mediated cGAMP import represents a general or cell type-specific mechanism.

The dominant import role of LRRC8A:C observed in TIME cells, an immortalized microvasculature endothelial lineage, strongly suggested that cGAMP import in primary human endothelial cells could also occur through LRRC8A channels. siRNA knockdown in primary human umbilical vein endothelial cells (HUVEC) decreased LRRC8A protein levels by ~70-90% (Figure 7A). As predicted, all siRNA treatments decreased extracellular cGAMP signaling, with oligo-9, -10, and -11 knocking down p-IRF3 signaling more than 50%. These results demonstrate that the LRRC8A channel is not

only the dominant cGAMP importer in immortalized human microvasculature cells, but also in primary HUVECs, and possibly in human tumor vasculature.

Given the modulation of LRRC8A-mediated cGAMP import that we achieved using S1P and DCPIB in the microvasculature line, we tested whether these same tools could effectively regulate cGAMP import in primary human endothelial cells. Consistent with our earlier findings, extracellular cGAMP signaling was increased in HUVEC cells by up to 1.4-fold in the presence of physiological S1P concentrations (Figure 7B). DCPIB again inhibited both basal and S1P-potentiated cGAMP import. These results establish pharmacologic modulation of the LRRC8A channel as a potential strategy to control cGAMP import into human vasculature.

Numerous immune cell types respond to cGAMP and cGAMP analogs, including monocytes/macrophages, dendritic cells, NK cells, and T cells[33]. We therefore sought to test whether the LRRC8A channel plays a major role in cGAMP import across major human immune subsets. To survey many cell types in parallel, we treated PBMCs with cGAMP with or without the LRRC8A channel inhibitor DCPIB. We then stained for p-STING together with cell lineage markers and assessed signaling activation by flow cytometry (Figure 7C and S6A). As expected, extracellular cGAMP treatment led to detection of p-STING in most subsets. Larger percentages of monocyte and dendritic cell populations responded to cGAMP compared to NK and T cell lineages, consistent with trends observed for STING agonist cytokine induction in murine immune subsets[33]. However, we did not observe any remarkable inhibitory effect of DCPIB in any subset.

Instead, a minor increase in p-STING was observed in $CD14^+$ PBMCs in both donors, which suggests that i) these cells use another unidentified importer and ii) the LRRC8A channel might play a minor role as a cGAMP exporter in these cells. Although it is possible that environmental or activating factors may upregulate usage of this import mechanism, these data imply that LRRC8A is not a major cGAMP importer in resting, circulating PBMCs.

The potential cell type-specificity of LRRC8A-mediated cGAMP transport holds important implications for the goal of modulating extracellular cGAMP signaling differentially. Therefore, we sought to confirm and expand upon the finding that LRRC8A does not appear to play a major import role in immune cells, especially T cells. Among primary immune subsets, VRAC has been predominantly studied in T cells. VRAC currents were first observed in human lymphocytes[70,71] and an LRRC8A-dependent, DCPIB-inhibited current, although low in magnitude, can be measured upon hypotonic stimulation of T cells[39]. Relative to other leukocytes, T cells express *LRRC8A* transcripts at higher levels, although it should be noted that PBMCs and the immune compartment have lower levels of *LRRC8A* compared to many other tissues (HumanProteinAtlas.com) (Figure S6B). We observed that isolated $CD3^+$ T cells respond weakly to extracellular cGAMP compared to primary endothelial cells (EC_{50} > 400 μM and EC_{50} ~ 43 μM, respectively, Figure S6C and S6D). This is consistent with previous reports that T cells weakly respond to extracellular cGAMP, but robustly respond to virally-packaged cGAMP, indicating that the T cell response is limited by cGAMP import[35]. Possible explanations include that T cells do not express potent

cGAMP importers at sufficient levels or that importers are inactive. Since T cells express receptors for S1P and can migrate in response to increasing S1P concentrations[63], we hypothesized that physiologic levels of S1P may increase LRRC8A's role in cGAMP import in T cells, similar to what we observed in vascular lineages. Treatment of $CD3^+$ T cells with extracellular cGAMP in the presence of S1P did not result in clear increases in STING signaling and the presence of DCPIB did not result in any clear inhibitory effect (Figure S6E). Collectively, we conclude that LRRC8A does not represent a dominant cGAMP import mechanism for T cells in this context, and more broadly for PBMCs. Therefore, among cell types that are known to play important roles in STING-dependent cGAMP detection, primary endothelial cells, but not PBMCs, use LRRC8A channels to import cGAMP.

DISCUSSION

Here we report identification of the LRRC8A:C heteromeric channel as the second known cGAMP transporter. The LRRC8 family was recently discovered to form the channels responsible for VRAC activity after three decades of active searching[39,40,70]. With the molecular identity of this channel now known, detailed mechanistic studies are now possible. Beyond small anions, LRRC8A channels transport metabolites, neurotransmitters, and small molecule drugs[48,50,52]. It is becoming clear that VRAC's namesake function in regulation of cell volume represents only a subset of the broad physiological roles these channels play. LRRC8A has been linked to cellular development, migration, and apoptosis, as well as cell-to-cell communication by regulating insulin release and mediating excitatory astrocyte-neuron signaling[41,45].

Through genetic, pharmacologic, and electrophysiological approaches, we identified a new class of substrates transported by this channel: immunostimulatory 2'3'-cyclic dinucleotides. This discovery opens new areas of inquiry as to the relationship between LRRC8A biology and cGAMP-STING innate immune signaling.

Once the LRRC8A channel is open, cGAMP travels down its chemical gradient across the plasma membrane. Indeed, other than serving as a cGAMP importer, we demonstrated that the LRRC8A channel, when activated, exports cGAMP out of HEK cells that overexpress cGAS. Therefore, LRRC8A is the first reported cGAMP exporter. In $CD14^+$ monocytes we observed a noteworthy effect in which treatment with the LRRC8A inhibitor DCPIB resulted in increased cGAMP signaling, hinting that the channel may act as an exporter in monocytes. The role that the LRRC8A channel plays as an exporter in cell types with high endogenous cGAMP warrants further investigation.

Identification of this new substrate class for LRRC8A channels also raises the question of how one family of channels can have such versatile roles. This is because the subunit composition of LRRC8A heteromeric complexes dictates the substrate specificity and physiologic role of each channel. Here, we demonstrated that LRRC8C, when complexed with the obligatory LRRC8A subunit, directly transports cGAMP. While LRRC8C and LRRC8E exhibit high homology[72], expression of LRRC8E is restricted. We observed little to no role for LRRC8E in cGAMP transport; however, it is conceivable that LRRC8A:E complexes could contribute to CDN transport when

sufficiently abundant. The presence of LRRC8D inhibits cGAMP transport, possibly because it forms non-productive complexes with LRRC8A or LRRC8A:C. Given the requirement of a specific LRRC8A heteromeric complex and differential expression profiles of the paralogs across cell types, we noticed that human vasculature cells express high levels of *LRRC8A* and *LRRC8C*, but low levels of *LRRC8D*. Indeed, an immortalized microvasculature cell line and primary human endothelial cells use LRRC8A channels as a dominant cGAMP import mechanism. In contrast, this channel does not seem to be a major importer in PBMCs, including $CD14^+$ monocytes and $CD3^+$ T cells.

Our identification of the dominant cGAMP importer in endothelial cells provides a molecular mechanism for sensing of 2'3'-CDNs by vasculature. Tumor vasculature was first reported to be the primary target of the mouse-specific STING agonist, DMXAA[73,74]. It was also shown to be a primary source of IFN-β production in response to intratumoral injections of cGAMP[34]. Upon STING activation, endothelial cells not only produce potent cytokines, but likely also mediate trafficking and egress of immune effector cells. However, STING activation is not beneficial in all cell types—high levels of STING signaling induce apoptosis or non-proliferative states in T cells[9,35–37], which is not desirable for eliciting cytotoxic T cell-mediated tumor clearance[38]. These results highlight the need for tight control of extracellular cGAMP-STING signaling in therapeutic applications. It is therefore advantageous that different responder cell types import extracellular cGAMP using distinct importers. An ideal anti-cancer cGAMP analog should take advantage of importer selectivity towards subtle structural

differences in CDNs to preferentially target beneficial cell types. Finally, we predict that further opening of the LRRC8A:C channel using pharmacological tools, including natural or synthetic S1P receptor agonists, would enhance the anti-cancer activity of extracellular cGAMP mediated by tumor vasculature. Conversely, inhibiting LRRC8A channels could block cGAMP transport to attenuate unwanted STING pathway activation in autoimmunity and inflammation.

ACKNOWLEDGMENTS

We thank all Li Lab members, Peter S. Kim, and Rajat Rohatgi for insightful comments and discussion throughout the course of this study. Flow cytometry analysis for this project was done on instruments in the Stanford Shared FACS Facility. Data was collected on an instrument in the Shared FACS Facility obtained using NIH S10 Shared Instrument Grant S10RR027431-01. L.J.L. thanks the Stanford Graduate Fellowship, ARCS Foundation, and Kimball Foundation for support. This research was supported by the National Institutes of Health grants DP2CA228044 (L.L.), DP2HD084069 (M.C.B.), and DOD grant W81XWH-18-1- 0041 (L.L.).

AUTHOR CONTRIBUTIONS

All authors designed the studies and discussed the findings in the manuscript. L.J.L., X.W., R.E.M., V.B., and G.T.H. performed experiments and analyzed data. C.R. and J.A.C. provided technical support. L.J.L. and L.L. wrote the manuscript.

DECLARATION OF INTERESTS

The authors declare no competing interests.

EXPERIMENTAL METHODS

Cell culture

Unless otherwise noted, cell lines were obtained from ATCC. U937 cells were maintained in RPMI (Cellgro) supplemented with 10% heat-inactivated FBS (Atlanta Biologicals) and 1% penicillin-streptomycin (Gibco). HEK293 cells were maintained in DMEM (Cellgro) supplemented with 10% FBS and 1% penicillin-streptomycin. Telomerase-immortalized human microvascular endothelium (TIME) cells line were maintained in vascular cell basal media supplemented with microvasculature endothelial cell growth kit-VEGF (ATCC) and 0.1% penicillin-streptomycin. Human umbilical vein endothelial cells (HUVEC) pooled from multiple donors were purchased from Lonza and maintained in EGM-2 supplemented growth media (Lonza). Primary human total T cells were maintained in RPMI supplemented with 10% heat-inactivated FBS, 1% penicillin-streptomycin, and 30 U/mL rhIL-2 (PeproTech). All cells were maintained in a 5% CO_2 incubator at 37 °C.

Reagents and antibodies

2'3'-cyclic-GMP-AMP (cGAMP) was synthesized and purified in-house as previously described[29]. 2'3'-bisphosphorothioate-cyclic-GMP-AMP (2'3'-cG^{S}A^{S}MP), 2'3'-cyclic-di-AMP (2'3'-CDA), 2'3'-bisphosphorothioate-cyclic-di-AMP (2'3'-CDA^S), 3'3'-cyclic-GMP-AMP (3'3'-cGAMP), 3'3'-cyclic-di-AMP (3'3'-CDA), and 3'3'-cyclic-di-GMP (3'3'-CDG) were purchased from Invivogen and reconstituted in endotoxin-free water. Sphingosine-

1-phosphate (d18:1) was purchased from Cayman Chemical. 4-[(2-Butyl-6,7-dichloro-2-cyclopentyl-2,3-dihydro-1-oxo-1*H*-inden-5-yl)oxy] butanoic acid (DCPIB) was purchased from Tocris Bioscience and reconstituted to 50 mM in DMSO. Antibodies and dilutions used for Western blotting or flow cytometry analysis are listed in Table S1.

Generation of CRISPR edited cell lines

LentiCRISPR v2 (Addgene) was used as the 3rd-generation lentiviral backbone for all knockout lines. Sequences for all sgRNAs used in this study are listed in Table S2. The guide sequences were cloned into the lentiviral backbone using the Lentiviral CRISPR Toolbox protocol from the Zhang Lab at MIT[76,77]. Lentiviral packaging plasmids (pHDM-G, pHDM-Hgmp2, pHDM-tat1b, and RC/CMV-rev1b) were purchased from Harvard Medical School. 500 ng of the lentiviral backbone plasmid containing the guide sequence and 500 ng of each of the packaging plasmids were transfected into HEK 293T cells using FuGENE 6 transfection reagent (Promega). The viral media was exchanged after 24 hours, harvested after 48 hours and passed through a 0.45 μm filter. U937 cells were transduced by spin infection in which cells were suspended in viral media with 8 μg/mL polybrene (Sigma Aldrich), centrifuged at 1000 x g for 1 hour, then resuspended in fresh media. HEK293 and TIME cell lines were reverse transduced by trypsinizing adherent cells and adding cell suspensions to viral media supplemented with 8 μg/mL polybrene. All lines were put under relevant antibiotic selection beginning 72-hours post-transduction and lasting until control (untransduced) cells completely died.

Cell viability measurement

U937 cells were treated with the indicated concentrations of cGAMP for 24 or 48 hours in duplicate. Cell density and viability was determined by hemocytometer and trypan blue staining.

U937 *SLC19A1*$^{-/-}$ CRISPR knockout library generation

Design of the whole-genome CRISPR sgRNA library was previously described by Morgens et al. (2017). Briefly, a whole-genome library of exon-targeting sgRNAs were designed, with the goal of minimizing off-target effects and maximizing gene disruption. The top 10 sgRNA sequences for each gene were included in the library, along with thousands of safe-targeting and non-targeting negative controls. The library was cloned into a lentiviral vector, pMCB320, which also expresses mCherry and a puromycin resistance cassette. The U937 Cas9-*SLC19A1*$^{-/-}$ line was generated by lentiviral transduction as described above. Knockout of *SLC19A1* was confirmed by genomic DNA sequencing (Figure S1A) and Cas9 function was confirmed by the efficiency of knocking out GFP expression using a sgRNA sequence against GFP confirmed by using a sgRNA sequence against GFP (Figure S1B). U937 Cas9-*SLC19A1*$^{-/-}$ cells were infected with the lentiviral CRISPR sgRNA library and selected with puromycin.

CRISPR screen

The U937 CRISPR knockout library line was grown in 4 spinner flasks (1 L), with 2 flasks serving as untreated controls and 2 flasks receiving cGAMP treatment. Throughout the screen all of the samples were split daily to keep the cell density at 250

million cells per 500 mL, which corresponded to 1,000 cells per guide in the untreated samples. The experimental samples were treated daily with enough cGAMP to reduce treated cell fold growth by 50% as compared to the control samples. Initial treatments began at 15 μM for two days and were then titrated to 30 μM. After a difference of ten population doublings was achieved between experimental and control samples (12 days), the genomic DNA was extracted using a Qiagen Blood Maxi Kit. The library was sequenced using a NextSeq 500/550 Mid Output v2 kit (Illumina). The experimental and control samples were compared using casTLE[44], available at https://bitbucket.org/dmorgens/castle. The algorithm determines the likely effect size for each gene, as well as the statistical significance of this effect.

Sequencing of gDNA to confirm CRISPR editing

gDNA was isolated from cell lines using the QIAamp DNA Mini Kit (Qiagen). Sequences of each gene loci flanking the sgRNA target sequence were PCR amplified. PCR products were purified and submitted for Sanger sequencing analysis. Control (unedited) and experimental (edited) sequence traces were analyzed using the Inference of CRISPR Edits (ICE) version2 software tool (Synthego). ICE knockout scores represent the proportion of sequences in which a coding frameshift or >21-bp insertion/deletion are detected.

Electroporation of STING agonists

U937 cells were resuspended in 100 μL electroporation solution (90 mM Na_2HPO_4, 90 mM NaH_2PO_4, 5 mM KCl, 10 mM $MgCl_2$, 10 mM sodium succinate) with the appropriate

concentration of STING agonist. Cells were then transferred to a cuvette with a 0.2 cm electrode gap (Bio-Rad) and electroporated using program U-013 on a Nucleofector II device (Lonza). Following electroporation, cells were transferred to media and cultured as indicated. Cell lysates were then harvested for analysis.

Stimulation of cGAMP synthesis and measurement of export in HEK293 cells

HEK293 cell lines were seeded in PurCol-coated (Advanced BioMatrix) 6-well plates at 300,000 total cells in 2 mL media one day before transfection. At the start of the experiment, media was gently removed and replaced with complete DMEM supplemented with ENPP1 inhibitor STF-1084 for 50 μM final. Cells were then transfected with 1500 ng pcDNA-FLAG-HA-sscGAS plasmid complexed with FuGene 6 reagent (Promega) according to manufacturer's instructions or treated with FuGene 6 alone as a negative control. After 24 hours of incubation, media from each condition was harvested and cells were immediately incubated for 20 minutes with hypotonic buffer (60 mM NaCl, 6 mM KCl, 1 mM $MgCl_2$, 1.5 mM $CaCl_2$, 10 mM glucose, 10 mM HEPES, pH 7.4, 155 mOsm). Following collection of buffer, media and buffer samples were centrifuged at 1000 x g for 10 minutes and supernatants collected. Extraction of cGAMP was then performed using HyperSep Aminopropyl SPE columns (ThermoFisher Scientific) and sample submitted for mass spectrometry quantification of cGAMP as previously described[28].

Electrophysiology

Endogenous VRAC currents from HEK293 cells were measured by whole-cell patch-clamp. Cells were transferred from culture dishes to the electrophysiology recording chamber following treatment with 0.5 mg/mL trypsin (Sigma-Aldrich) for 2 minutes. External recording solution contained 88 mM NaCl, 10 mM HEPES with either 110 mM mannitol (isotonic, 300 mOsm/kg) or 30 mM mannitol (hypotonic, 230mOsm/kg), pH 7.4 by NaOH. The internal (pipette) solution contained 130 mM CsCl, 10 mM HEPES, 4 mM Mg-ATP, pH 7.3. Borosilicate glass micropipettes (Sutter Instruments, Novato, CA) were pulled and fire-polished to a tip diameter with a typical resistance of 1.5–3.0 MΩ. Data were acquired using an Axopatch-200B amplifier (Axon Instruments, Union City, CA) and InstruTECH ITC-16 interface (HEKA Instruments, Holliston, MA), with a sampling rate of 5 kHz and filtering at 1 kHz. Igor Pro (WaveMetrics, Portland, OR) software was used for stimulation and data collection. Currents were measured in response to voltage ramps from −150 to 150 mV over 1.0 s, with an inter-ramp interval of 10 s and a holding potential of 0 mV. All recordings were carried out at room temperature (20 – 22 ºC).

Lipofection of cGAMP

Lipofectamine 3000 (Thermo Fisher Scientific) was diluted into Opti-MEM (3 µL into 50 µL), P3000 was diluted into Opti-MEM (2 µL into 50 uL) in the absence or presence of cGAMP (for 1 µM final in experiment), and then dilutions were combined and incubated for 15 minutes. Lipid complexes (100 µL) were added dropwise to plated cells in 900 uL media. In parallel, free cGAMP was added for 1 µM final in the absence of lipid reagent.

Inducible expression of LRRC8A and LRRC8C

Gene fragments encoding LRRC8A (Uniprot Q8IWT6) and LRRC8C (Uniprot Q8TDW0) were commercially synthesized and cloned into plasmids (Twist Bioscience). Synonymous DNA mutations were introduced by QuickChange to ablate downstream Cas9-sgRNA targeting at each site (LRRC8A: GGATCCTGAAGCCGTGGT to GCATTTTAAAACCATGGT, LRRC8C: GTTATGAGCGAGCCCTCCAC to GCTACGAACGCGCGTTACAT). Additionally, QuickChange was used to generate a sequence with a LRRC8A-R103L encoding substitution (CGG to CTG). A parent pLVX-TetOne plasmid (Takara Bio) was modified by 1) insertion of a GGSG-FLAG encoding sequence to flank the multiple cloning site and 2) insertion of SV40 promoter and hygromycin resistance factor encoding sequences were cloned in following the TetOn 3G element, yielding a pLVX-TetOne-FLAG-Hygro plasmid. LRRC8A, LRRC8A-R103L, and LRRC8C DNA fragments (all with ablated sgRNA sites) were then cloned into pLVX-TetOne-FLAG-Hygro backbone by Gibson assembly. Lentiviral packaging of constructs was performed as described above and reverse transduced into LRRC8A$^{-/-}$ or LRRC8C$^{-/-}$ TIME cells. Cells were selected with hygromycin for 2 weeks. Doxycycline was added to cultures for 36 hours at the indicated concentrations before each experiment to induce expression.

S1P RECONSTITUTION

Lipid was solubilized in warm methanol, aliquoted, then solvent evaporated under nitrogen before storage at -20*C. At the start of each experiment, S1P was freshly

reconstituted to 100 μM with 4 mg/mL fatty acid-free human serum albumin carrier protein (Millipore Sigma) in PBS.

siRNA knockdown of *LRRC8A* in HUVEC

Four ON-TARGETplus siRNAs for knockdown of *LRRC8A* were purchased from Dharmacon, along with non-targeting control siRNA. HUVEC cells were seeded the night before transfection in 6-well plates at $2.5x10^5$ total cells in 2 mL media, with a change to fresh media on the day of knockdown. Following manufacturer's instructions DharmaFECT4 (6 uL) was complexed with siRNA (10 uL of 5 uM stock) in Opti-MEM to yield 200 uL of complexes then used to transfect cells. Cells were split on day three post-transfection and tested for cGAMP response on day four.

PBMC isolation and purification of $CD3^+$ cell subsets

Human peripheral blood was collected as a buffy coat (Stanford Blood Center). Mononuclear cells were purified by density gradient centrifugation over Ficoll-Paque Premium (1.077 g/mL, GE Healthcare) in Leukosep tubes (Grenier Bio-One) according to manufacturer protocol. $CD3^+$ T cells were purified from PBMCs by negative selection using a Pan T Cell Isolation Kit (Miltenyi Biotec) following manufacturer's instructions.

Flow cytometry analysis of PBMCs

Cells were stained with LIVE/DEAD Fixable Blue Dead Cell Stain (ThermoFisher) and then fixed/permeabilized using the eBioscience Foxp3/Transcription Factor Staining Buffer Set (Invitrogen) according to manufacturer protocols. Antibody panel design was

based on a previously reported panel (OMIP-042) designed for immunophenotyping of major PBMC subsets[75]. Cells were antibody-stained for p-STING, CD14, HLA-DR, CD56, CD20, CD4, CD8, CD3, and CD123 using the reagents and dilutions detailed in Table S1. Cell staining was measured using an Aurora (Cytek) flow cytometer, with resulting data analyzed using FlowJo V10 software (Treestar).

Statistical analysis

All statistical analyses were performed using GraphPad Prism 8.3.1. For all experiments involving Western blots, densitometric measurements of protein bands were made using ImageJ 1.52a. For comparison of values attained within one blot (Figure 2A), significance was calculated by two-tailed *t*-test, assuming a Gaussian distribution. In cases where biological replicates of independent experiments represent paired sets of blots (Figures 3-5), significance was calculated by ratio paired *t*-test assuming a Gaussian distribution.

REFERENCES

1. Wu, J., Sun, L., Chen, X., Du, F., Shi, H., Chen, C., and Chen, Z.J. (2013). Cyclic GMP-AMP is an endogenous second messenger in innate immune signaling by cytosolic DNA. Science *339*, 826–830.

2. Ablasser, A., Goldeck, M., Cavlar, T., Deimling, T., Witte, G., Röhl, I., Hopfner, K.-P., Ludwig, J., and Hornung, V. (2013). cGAS produces a 2'-5'-linked cyclic dinucleotide second messenger that activates STING. Nature *498*, 380–384.

3. Diner, E.J., Burdette, D.L., Wilson, S.C., Monroe, K.M., Kellenberger, C.A., Hyodo, M., Hayakawa, Y., Hammond, M.C., and Vance, R.E. (2013). The innate immune DNA sensor cGAS produces a noncanonical cyclic dinucleotide that activates human STING. Cell Reports *3*, 1355–61.

4. Zhang, X., Shi, H., Wu, J., Zhang, X., Sun, L., Chen, C., and Chen, Z.J. (2013).

Cyclic GMP-AMP containing mixed phosphodiester linkages is an endogenous high-affinity ligand for STING. Mol Cell *51*, 226–35.

5. Gao, P., Ascano, M., Wu, Y., Barchet, W., Gaffney, B.L., Zillinger, T., Serganov, A.A., Liu, Y., Jones, R.A., Hartmann, G., et al. (2013). Cyclic [G(2',5')pA(3',5')p] is the metazoan second messenger produced by DNA-activated cyclic GMP-AMP synthase. Cell *153*, 1094–107.

6. Li, X.-D., Wu, J., Gao, D., Wang, H., Sun, L., and Chen, Z.J. (2013). Pivotal roles of cGAS-cGAMP signaling in antiviral defense and immune adjuvant effects. Science *341*, 1390–1394.

7. Gao, D., Li, T., Li, X.-D., Chen, X., Li, Q.-Z., Wight-Carter, M., and Chen, Z.J. (2015). Activation of cyclic GMP-AMP synthase by self-DNA causes autoimmune diseases. Proceedings of the National Academy of Sciences of the United States of America *112*, E5699-705.

8. Manzanillo, P.S., Shiloh, M.U., Portnoy, D.A., and Cox, J.S. (2012). Mycobacterium tuberculosis activates the DNA-dependent cytosolic surveillance pathway within macrophages. Cell host & microbe *11*, 469–480.

9. Nandakumar, R., Tschismarov, R., Meissner, F., Prabakaran, T., Krissanaprasit, A., Farahani, E., Zhang, B.-C., Assil, S., Martin, A., Bertrams, W., et al. (2019). Intracellular bacteria engage a STING-TBK1-MVB12b pathway to enable paracrine cGAS-STING signalling. Nature microbiology *4*, 701–713.

10. Harding, S.M., Benci, J.L., Irianto, J., Discher, D.E., Minn, A.J., and Greenberg, R.A. (2017). Mitotic progression following DNA damage enables pattern recognition within micronuclei. Nature *548*, 466–470.

11. Hatch, E.M., Fischer, A.H., Deerinck, T.J., and Hetzer, M.W. (2013). Catastrophic nuclear envelope collapse in cancer cell micronuclei. Cell *154*, 47–60.

12. McArthur, K., Whitehead, L.W., Heddleston, J.M., Li, L., Padman, B.S., Oorschot, V., Geoghegan, N.D., Chappaz, S., Davidson, S., Chin, H., et al. (2018). BAK/BAX macropores facilitate mitochondrial herniation and mtDNA efflux during apoptosis. Science *359*, eaao6047.

13. Bakhoum, S.F., Ngo, B., Laughney, A.M., Cavallo, J.-A., Murphy, C.J., Ly, P., Shah, P., ram, R.K., Watkins, T.B., Taunk, N.K., et al. (2018). Chromosomal instability drives metastasis through a cytosolic DNA response. Nature *553*, 467–472.

14. Mackenzie, K.J., Carroll, P., Martin, C.-A., Murina, O., Fluteau, A., Simpson, D.J., Olova, N., Sutcliffe, H., Rainger, J.K., Leitch, A., et al. (2017). cGAS surveillance of micronuclei links genome instability to innate immunity. Nature *548*, 461–465.

15. Dou, Z., Ghosh, K., Vizioli, M., Zhu, J., Sen, P., Wangensteen, K.J., Simithy, J., Lan, Y., Lin, Y., Zhou, Z., et al. (2017). Cytoplasmic chromatin triggers inflammation in senescence and cancer. Nature *550*, 402–406.

16. Glück, S., Guey, B., Gulen, M., Wolter, K., Kang, T.-W., Schmacke, N., Bridgeman, A., Rehwinkel, J., Zender, L., and Ablasser, A. (2017). Innate immune sensing of cytosolic chromatin fragments through cGAS promotes senescence. Nature cell biology *19*, 1061–1070.

17. Yang, H., Wang, H., Ren, J., Chen, Q., and Chen, Z.J. (2017). cGAS is essential for cellular senescence. Proceedings of the National Academy of Sciences of the United States of America *114*, E4612–E4620.

18. Tanaka, Y., and Chen, Z.J. (2012). STING specifies IRF3 phosphorylation by TBK1 in the cytosolic DNA signaling pathway. Sci Signal *5*, ra20.

19. Liu, S., Cai, X., Wu, J., Cong, Q., Chen, X., Li, T., Du, F., Ren, J., Wu, Y.-T., Grishin, N.V., et al. (2015). Phosphorylation of innate immune adaptor proteins MAVS, STING, and TRIF induces IRF3 activation. Sci New York N Y *347*, aaa2630.

20. Zhong, B., Yang, Y., Li, S., Wang, Y.-Y., Li, Y., Diao, F., Lei, C., He, X., Zhang, L., Tien, P., et al. (2008). The Adaptor Protein MITA Links Virus-Sensing Receptors to IRF3 Transcription Factor Activation. Immunity *29*, 538–550.

21. Sun, L., Wu, J., Du, F., Chen, X., and Chen, Z.J. (2013). Cyclic GMP-AMP synthase is a cytosolic DNA sensor that activates the type I interferon pathway. Science *339*, 786–791.

22. Stetson, D.B., Ko, J.S., Heidmann, T., and Medzhitov, R. (2008). Trex1 prevents cell-intrinsic initiation of autoimmunity. Cell *134*, 587–598.

23. Crowl, J.T., Gray, E.E., Pestal, K., Volkman, H.E., and Stetson, D.B. (2017). Intracellular Nucleic Acid Detection in Autoimmunity. Annu Rev Immunol *35*, 313–336.

24. Sliter, D.A., Martinez, J., Hao, L., Chen, X., Sun, N., Fischer, T.D., Burman, J.L., Li, Y., Zhang, Z., Narendra, D.P., et al. (2018). Parkin and PINK1 mitigate STING-induced inflammation. Nature *561*, 258–262.

25. Ablasser, A., Schmid-Burgk, J.L., Hemmerling, I., Horvath, G.L., Schmidt, T., Latz, E., and Hornung, V. (2013). Cell intrinsic immunity spreads to bystander cells via the intercellular transfer of cGAMP. Nature *503*, 530–534.

26. Bridgeman, A., Maelfait, J., Davenne, T., Partridge, T., Peng, Y., Mayer, A., Dong, T., Kaever, V., Borrow, P., and Rehwinkel, J. (2015). Viruses transfer the antiviral second messenger cGAMP between cells. Science *349*, 1228–1232.

27. Gentili, M., Kowal, J., Tkach, M., Satoh, T., Lahaye, X., Conrad, C., Boyron, M., Lombard, B., Durand, S., Kroemer, G., et al. (2015). Transmission of innate immune signaling by packaging of cGAMP in viral particles. Science *349*, 1232–1236.

28. Carozza, J.A., Böhnert, V., Nguyen, K.C., Skariah, G., Shaw, K.E., Brown, J.A., Rafat, M., von Eyben, R., Graves, E.E., Glenn, J.S., et al. (2020). 2'3'-cGAMP is an immunotransmitter produced by cancer cells and regulated by ENPP1. Nature Cancer.

29. Ritchie, C., Cordova, A.F., Hess, G.T., Bassik, M.C., and Li, L. (2019). SLC19A1 Is an Importer of the Immunotransmitter cGAMP. Molecular cell.

30. Luteijn, R.D., Zaver, S.A., Gowen, B.G., Wyman, S.K., Garelis, N.E., Onia, L., McWhirter, S.M., Katibah, G.E., Corn, J.E., Woodward, J.J., et al. (2019). SLC19A1 transports immunoreactive cyclic dinucleotides. Nature *573*, 434–438.

31. Li, L., Yin, Q., Kuss, P., Maliga, Z., Millán, J.L., Wu, H., and Mitchison, T.J. (2014). Hydrolysis of 2'3'-cGAMP by ENPP1 and design of nonhydrolyzable analogs. Nature chemical biology *10*, 1043–1048.

32. Corrales, L., Glickman, L., McWhirter, S.M., Kanne, D.B., Sivick, K.E., Katibah, G.E., Woo, S.-R., Lemmens, E., Banda, T., Leong, J.J., et al. (2015). Direct Activation of STING in the Tumor Microenvironment Leads to Potent and Systemic Tumor Regression and Immunity. Cell reports *11*, 1018–1030.

33. Francica, B.J., Ghasemzadeh, A., Desbien, A.L., Theodros, D., Sivick, K.E., Reiner, G.L., Glickman, L., Marciscano, A.E., Sharabi, A.B., Leong, M.L., et al. (2018). TNFα and Radioresistant Stromal Cells Are Essential for Therapeutic Efficacy of Cyclic Dinucleotide STING Agonists in Nonimmunogenic Tumors. Cancer Immunol Res *6*, 422–433.

34. Demaria, O., Gassart, A., Coso, S., Gestermann, N., Domizio, J., Flatz, L., Gaide, O., Michielin, O., Hwu, P., Petrova, T.V., et al. (2015). STING activation of tumor endothelial cells initiates spontaneous and therapeutic antitumor immunity. Proceedings of the National Academy of Sciences of the United States of America *112*, 15408–15413.

35. Gulen, M.F., Koch, U., Haag, S.M., Schuler, F., Apetoh, L., Villunger, A., Radtke, F., and Ablasser, A. (2017). Signalling strength determines proapoptotic functions of STING. Nature Communications *8*, 427–10.

36. Larkin, B., Ilyukha, V., Sorokin, M., Buzdin, A., Vannier, E., and Poltorak, A. (2017). Cutting Edge: Activation of STING in T Cells Induces Type I IFN Responses and Cell Death. J Immunol *199*, 397–402.

37. Cerboni, S., Jeremiah, N., Gentili, M., Gehrmann, U., Conrad, C., Stolzenberg, M.-C., Picard, C., Neven, B., Fischer, A., Amigorena, S., et al. (2017). Intrinsic

antiproliferative activity of the innate sensor STING in T lymphocytes. J Exp Medicine *214*, 1769–1785.

38. Sivick, K.E., Desbien, A.L., Glickman, L., Reiner, G.L., Corrales, L., Surh, N.H., Hudson, T.E., Vu, U.T., Francica, B.J., Banda, T., et al. (2018). Magnitude of Therapeutic STING Activation Determines CD8+ T Cell-Mediated Anti-tumor Immunity. Cell Reports *25*, 3074-3085.e5.

39. Qiu, Z., Dubin, A.E., Mathur, J., Tu, B., Reddy, K., Miraglia, L.J., Reinhardt, J., Orth, A.P., and Patapoutian, A. (2014). SWELL1, a plasma membrane protein, is an essential component of volume-regulated anion channel. Cell *157*, 447–458.

40. Voss, F.K., Ullrich, F., Münch, J., Lazarow, K., Lutter, D., Mah, N., Andrade-Navarro, M.A., von Kries, J.P., Stauber, T., and Jentsch, T.J. (2014). Identification of LRRC8 heteromers as an essential component of the volume-regulated anion channel VRAC. Science *344*, 634–638.

41. Chen, L., König, B., Liu, T., Pervaiz, S., Razzaque, Y.S., and Stauber, T. (2019). More than just a pressure release valve: physiological roles of volume-regulated LRRC8 anion channels. Biological chemistry *0*.

42. Yang, J., Vitery, M., Chen, J., Osei-Owusu, J., Chu, J., and Qiu, Z. (2019). Glutamate-Releasing SWELL1 Channel in Astrocytes Modulates Synaptic Transmission and Promotes Brain Damage in Stroke. Neuron *102*, 813-827.e6.

43. Morgens, D.W., Wainberg, M., Boyle, E.A., Ursu, O., Araya, C.L., Tsui, K.C., Haney, M.S., Hess, G.T., Han, K., Jeng, E.E., et al. (2017). Genome-scale measurement of off-target activity using Cas9 toxicity in high-throughput screens. Nature Communications *8*, 15178.

44. Morgens, D.W., ans, R., Li, A., and Bassik, M.C. (2016). Systematic comparison of CRISPR/Cas9 and RNAi screens for essential genes. Nature Biotechnology *34*, 634–636.

45. Osei-Owusu, J., Yang, J., del Vitery, M., and Qiu, Z. (2018). Molecular Biology and Physiology of Volume-Regulated Anion Channel (VRAC). Current Topics in Membranes *81*, 177–203.

46. Strange, K., Yamada, T., and Denton, J.S. (2019). A 30-year journey from volume-regulated anion currents to molecular structure of the LRRC8 channel. The Journal of general physiology *151*, 100–117.

47. Gaitán-Peñas, H., Gradogna, A., Laparra-Cuervo, L., Solsona, C., Fernández-Dueñas, V., Barrallo-Gimeno, A., Ciruela, F., Lakadamyali, M., Pusch, M., and Estévez, R. (2016). Investigation of LRRC8-Mediated Volume-Regulated Anion Currents in Xenopus Oocytes. Biophysical journal *111*, 1429–1443.

48. Lutter, D., Ullrich, F., Lueck, J.C., Kempa, S., and Jentsch, T.J. (2017). Selective transport of neurotransmitters and modulators by distinct volume-regulated LRRC8 anion channels. Journal of cell science *130*, 1122–1133.

49. Syeda, R., Qiu, Z., Dubin, A.E., Murthy, S.E., Florendo, M.N., Mason, D.E., Mathur, J., Cahalan, S.M., Peters, E.C., Montal, M., et al. (2016). LRRC8 Proteins Form Volume-Regulated Anion Channels that Sense Ionic Strength. Cell *164*, 499–511.

50. Planells-Cases, R., Lutter, D., Guyader, C., Gerhards, N.M., Ullrich, F., Elger, D.A., Kucukosmanoglu, A., Xu, G., Voss, F.K., Reincke, M.S., et al. (2015). Subunit composition of VRAC channels determines substrate specificity and cellular resistance to Pt-based anti-cancer drugs. The EMBO journal *34*, 2993–3008.

51. Schober, A.L., Wilson, C.S., and Mongin, A.A. (2017). Molecular composition and heterogeneity of the LRRC8-containing swelling-activated osmolyte channels in primary rat astrocytes. The Journal of physiology *595*, 6939–6951.

52. Lee, C.C., Freinkman, E., batini, D., and Ploegh, H.L. (2014). The protein synthesis inhibitor blasticidin s enters mammalian cells via leucine-rich repeat-containing protein 8D. The Journal of biological chemistry *289*, 17124–17131.

53. Pedersen, S., Klausen, T., and Nilius, B. (2015). The identification of a volume-regulated anion channel: an amazing Odyssey. Acta Physiol *213*, 868–881.

54. Dunn, P.J., Salm, E.J., and Tomita, S. (2020). ABC transporters control ATP release through cholesterol-dependent volume-regulated anion channel activity. J Biological Chem, jbc.RA119.010699.

55. Hisadome, K., Koyama, T., Kimura, C., Droogmans, G., Ito, Y., and Oike, M. (2002). Volume-regulated anion channels serve as an auto/paracrine nucleotide release pathway in aortic endothelial cells. The Journal of general physiology *119*, 511–520.

56. Jackson, P., and Strange, K. (1995). Characterization of the voltage-dependent properties of a volume-sensitive anion conductance. The Journal of general physiology *105*, 661–676.

57. Tsumura, T., Oiki, S., Ueda, S., Okuma, M., and Okada, Y. (1996). Sensitivity of volume-sensitive Cl- conductance in human epithelial cells to extracellular nucleotides. Am J Physiol-cell Ph *271*, C1872–C1878.

58. Kefauver, J.M., Saotome, K., Dubin, A.E., Pallesen, J., Cottrell, C.A., Cahalan, S.M., Qiu, Z., Hong, G., Crowley, C.S., Whitwam, T., et al. (2018). Structure of the human volume regulated anion channel. eLife *7*, 551.

59. Woodhull, A.M. (1973). Ionic Blockage of Sodium Channels in Nerve. J Gen

Physiology *61*, 687–708.

60. Deneka, D., Sawicka, M., Lam, A.K., Paulino, C., and Dutzler, R. (2018). Structure of a volume-regulated anion channel of the LRRC8 family. Nature *558*, 254–259.

61. Kasuya, G., Nakane, T., Yokoyama, T., Jia, Y., Inoue, M., Watanabe, K., Nakamura, R., Nishizawa, T., Kusakizako, T., Tsutsumi, A., et al. (2018). Cryo-EM structures of the human volume-regulated anion channel LRRC8. Nature Structural & Molecular Biology *25*, 797–804.

62. Burow, P., Klapperstück, M., and Markwardt, F. (2014). Activation of ATP secretion via volume-regulated anion channels by sphingosine-1-phosphate in RAW macrophages. Pflügers Archiv European J Physiology *467*, 1215–26.

63. Cartier, A., and Hla, T. (2019). Sphingosine 1-phosphate: Lipid signaling in pathology and therapy. Science *366*, eaar5551-14.

64. Decher, N., Lang, H., Nilius, B., Brüggemann, A., Busch, A., and Steinmeyer, K. (2001). DCPIB is a novel selective blocker of I(Cl,swell) and prevents swelling-induced shortening of guinea-pig atrial action potential duration. British journal of pharmacology *134*, 1467–1479.

65. Kern, D.M., Oh, S., Hite, R.K., and Brohawn, S.G. (2019). Cryo-EM structures of the DCPIB-inhibited volume-regulated anion channel LRRC8A in lipid nanodiscs. eLife *8*, 551.

66. Burdette, D.L., Monroe, K.M., Sotelo-Troha, K., Iwig, J.S., Eckert, B., Hyodo, M., Hayakawa, Y., and Vance, R.E. (2011). STING is a direct innate immune sensor of cyclic di-GMP. Nature *478*, 515–8.

67. Woodward, J.J., Iavarone, A.T., and Portnoy, D.A. (2010). c-di-AMP secreted by intracellular Listeria monocytogenes activates a host type I interferon response. Sci New York N Y *328*, 1703–5.

68. Sauer, J.-D., Sotelo-Troha, K., von Moltke, J., Monroe, K.M., Rae, C.S., Brubaker, S.W., Hyodo, M., Hayakawa, Y., Woodward, J.J., Portnoy, D.A., et al. (2010). The N-ethyl-N-nitrosourea-induced Goldenticket mouse mutant reveals an essential function of Sting in the in vivo interferon response to Listeria monocytogenes and cyclic dinucleotides. Infect Immun *79*, 688–94.

69. Dey, B., Dey, R., Cheung, L.S., Pokkali, S., Guo, H., Lee, J.-H., and Bishai, W.R. (2015). A bacterial cyclic dinucleotide activates the cytosolic surveillance pathway and mediates innate resistance to tuberculosis. Nat Med *21*, 401–6.

70. Grinstein, S., Dupre, A., and Rothstein, A. (1982). Volume regulation by human lymphocytes. Role of calcium. J Gen Physiology *79*, 849–868.

71. Cahalan, and Lewis, R. (1988). Role of potassium and chloride channels in volume regulation by T lymphocytes. Soc Gen Phy *43*, 281–301.

72. Abascal, F., and Zardoya, R. (2012). LRRC8 proteins share a common ancestor with pannexins, and may form hexameric channels involved in cell-cell communication. BioEssays : news and reviews in molecular, cellular and developmental biology *34*, 551–560.

73. Conlon, J., Burdette, D.L., Sharma, S., Bhat, N., Thompson, M., Jiang, Z., Rathinam, V.A., Monks, B., Jin, T., Xiao, S.T., et al. (2013). Mouse, but not human STING, binds and signals in response to the vascular disrupting agent 5,6-dimethylxanthenone-4-acetic acid. J Immunol Baltim Md 1950 *190*, 5216–25.

74. Zwi, L., Baguley, B., Gavin, J., and Wilson, W. (1994). Correlation between immune and vascular activities of xanthenone acetic acid antitumor agents. Oncol Res *6*, 79–85.

75. Staser, K.W., Eades, W., Choi, J., Karpova, D., and DiPersio, J.F. (2018). OMIP-042: 21-color flow cytometry to comprehensively immunophenotype major lymphocyte and myeloid subsets in human peripheral blood. Cytometry. Part A : the journal of the International Society for Analytical Cytology *93*, 186–189.

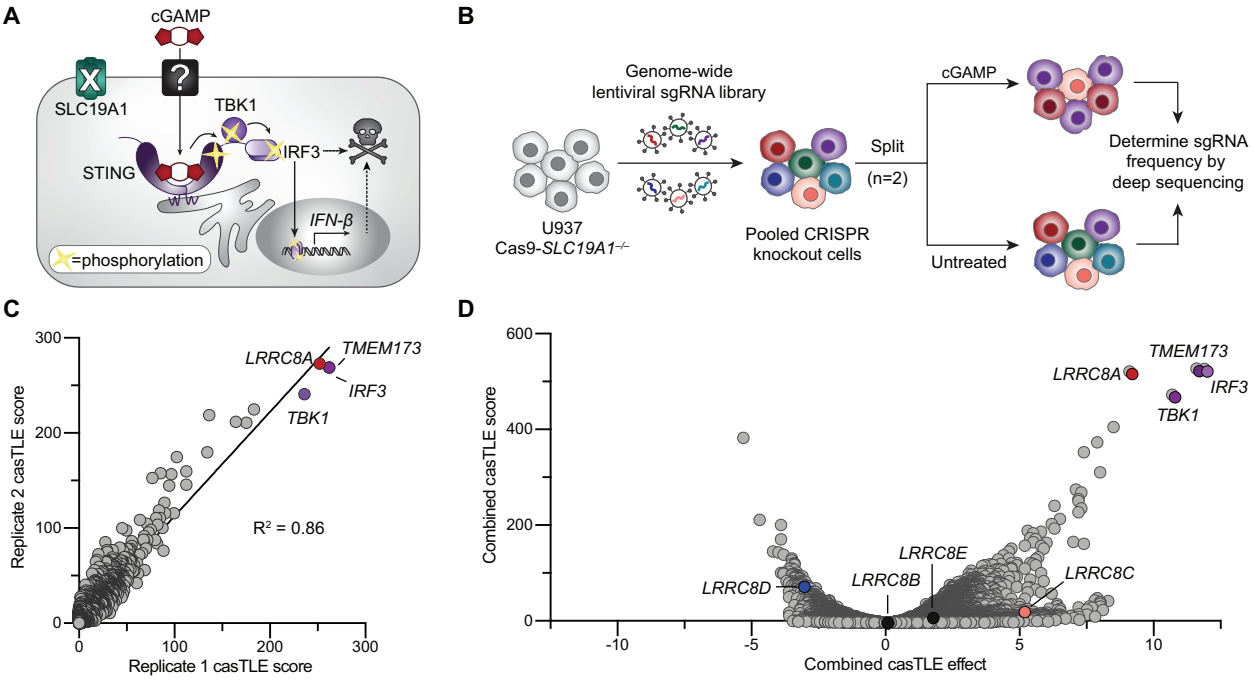

Figure 1. A Genome-Wide CRISPR Screen Identifies LRRC8A as a Positive Regulator of Extracellular cGAMP-Mediated STING Pathway Activation

(A) Scheme of extracellular cGAMP-STING signaling in U937 *SLC19A1*$^{-/-}$ cells. cGAMP imported from the extracellular space binds to and activates STING. The resulting signaling cascade leads to phosphorylation of STING, the kinase TBK1, and the transcription factor IRF3, ultimately leading to cytokine production and cell death.

(B) CRISPR screen strategy. U937 Cas9-*SLC19A1*$^{-/-}$ cells were transduced with a whole-genome sgRNA lentiviral library. In two replicates, library cells were treated with cGAMP or untreated for 12 days. Genomic DNA was harvested, deep sequenced, and analyzed for sgRNA depletion or enrichment.

(C) Plot of casTLE score for every gene in replicate 1 versus replicate 2 with displayed correlation across all genes (R^2 = 0.86). Top scoring hits are annotated.

(D) Volcano plot of casTLE effect size versus score for all genes across combined replicates. Top enriched hits, as well the *LRRC8* family, are annotated.

See also Figure S1.

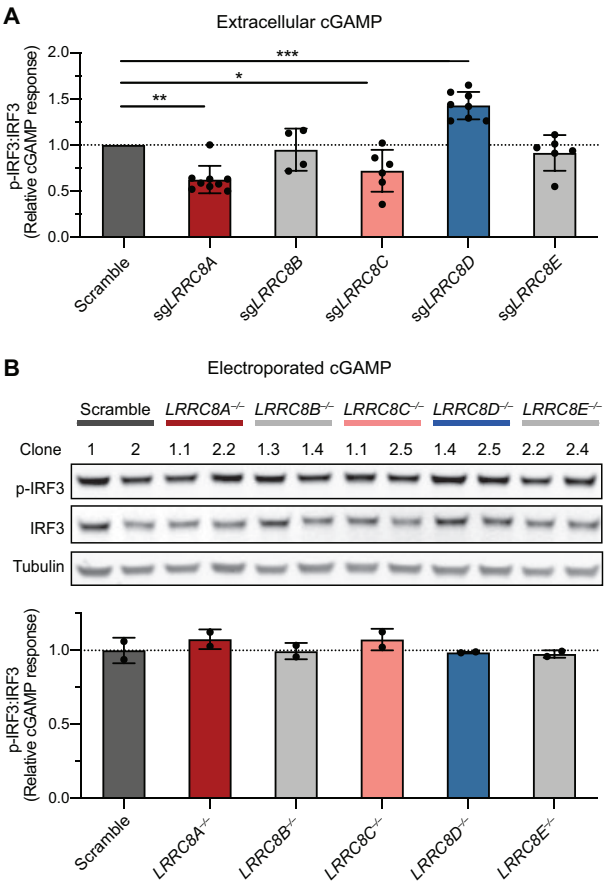

Figure 2. LRRC8A and LRRC8 Paralogs Differentially Facilitate cGAMP Import

(A) Effect of LRRC8A–E on extracellular cGAMP signaling. U937 *SLC19A1*$^{-/-}$ clones expressing scramble or *LRRC8A*–*LRRC8E* sgRNAs were treated with 100 μM cGAMP for 4 h and signaling was assessed by Western blot (see Figure S2). Summarized results for clones (confirmed heterozygous or homozygous knockout) are plotted relative to the respective scramble control average (n = 4–9 biological replicates). Significance calculated using two-tailed *t*-test; **P* ≤ 0.05, ***P* ≤ 0.01, ****P* ≤ 0.001.

(B) Effect of LRRC8A–LRRC8E on intracellular cGAMP signaling. U937 *SLC19A1*$^{-/-}$-scramble or -*LRRC8A*$^{-/-}$ through -*LRRC8E*$^{-/-}$ clones were electroporated with 100 nM cGAMP, cultured for 2 h, and assessed for signaling by Western blot (n = 2 biological replicates).

For (A)–(B), results plotted as mean ± SD. See also Figure S2.

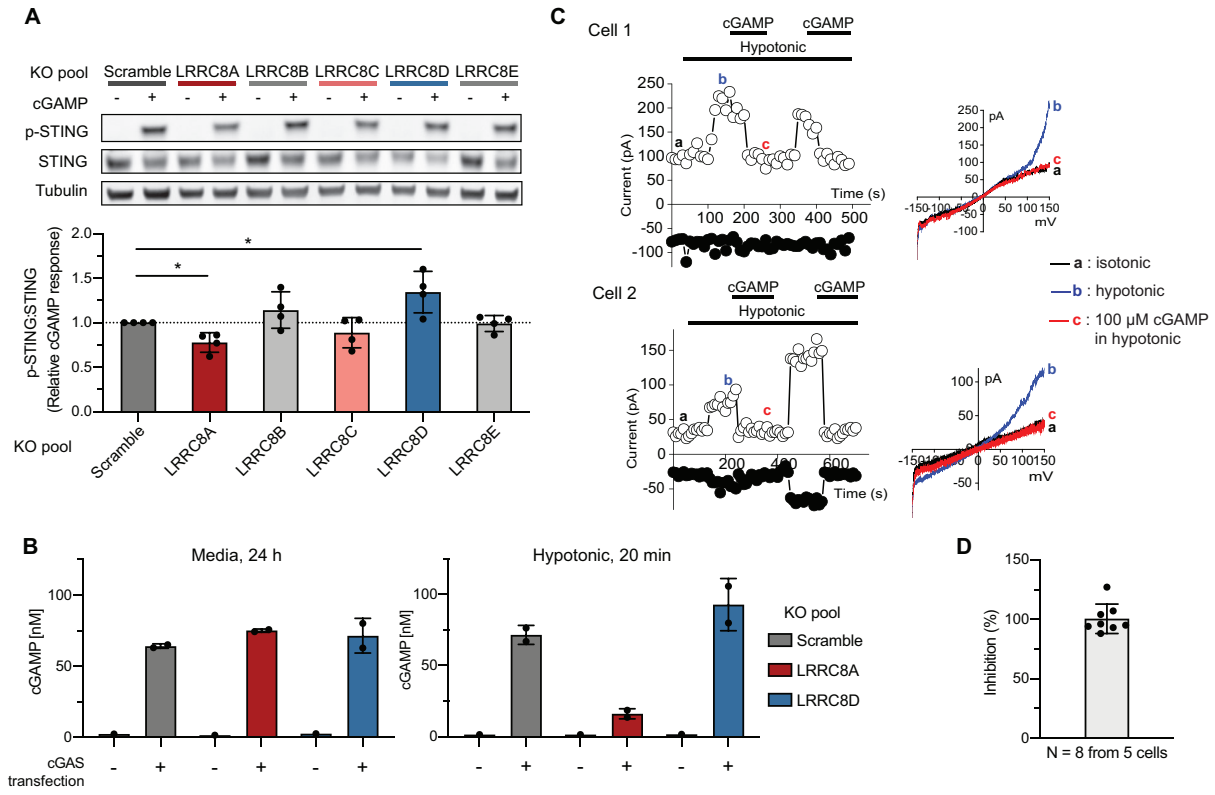

Figure 3. LRRC8A-Containing VRAC Channels Directly Transport cGAMP

(A) Effect of LRRC8A–E on extracellular cGAMP signaling in HEK293 cells. HEK293 scramble or LRRC8A–LRRC8E knockout pools were treated with 100 μM cGAMP for 2 h and signaling then assessed by Western blot. Representative blots displayed with quantification of all experiments (n = 4 biological replicates).

(B) Extracellular cGAMP concentrations from HEK293 scramble, LRRC8A, or LRRC8D knockout pools were measured by LC-MS/MS following cGAS plasmid transfection from media (24 h) or after hypotonic buffer stimulus (20 min) (n = 2 technical replicates).

(C) Representative whole-cell patch clamp current traces measured in HEK293 cells upon hypotonic stimulation in the absence or presence of cGAMP (100 μM). Overlays of the current-voltage relationship at the indicated points are also displayed. Additional traces from three separate cells are included in Figure S3.

(D) Summary data for inhibition of VRAC current by 100 μM extracellular cGAMP. Inhibition of the hypotonic-induced current at +150 mV is displayed (n = 8 measured in 5 cells from separate cover slips).

For (A), (B), and (D), data are mean ± SD. Significance calculated using ratio paired *t*-test; **P* ≤ 0.05. See also Figure S3.

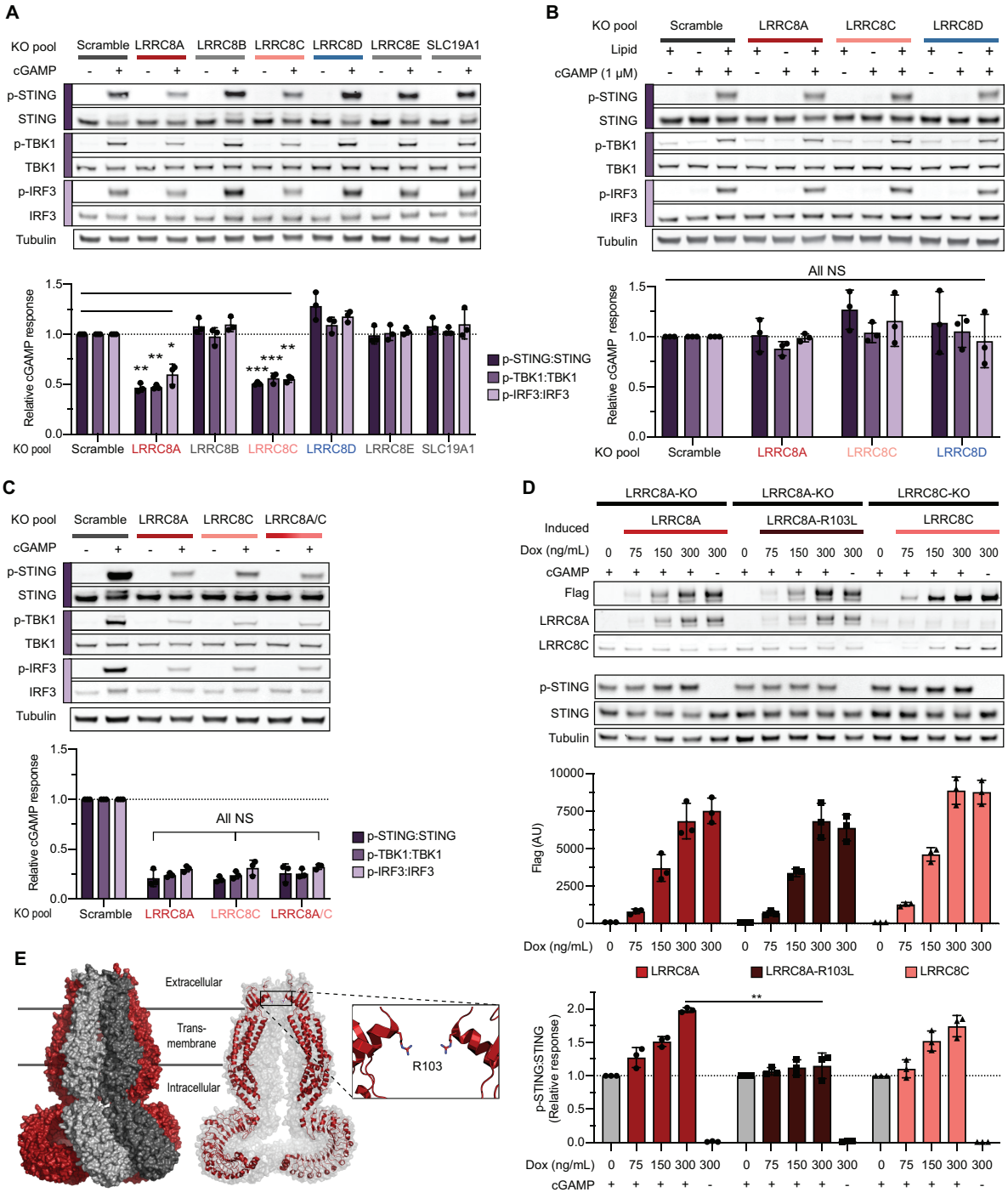

Figure 4. The LRRC8A:C Channel Is the Dominant cGAMP Importer in Microvasculature Cells

(See next page for full figure legend)

Figure 4. The LRRC8A:C Channel Is the Dominant cGAMP Importer in Microvasculature Cells

(A) Effect of LRRC8A–E and SLC19A1 on extracellular cGAMP signaling in TIME cells. Knockout pools were treated with 50 μM cGAMP for 2 h and signaling then assessed by Western blot (n = 3 biological replicates).

(B) Effect of LRRC8A, LRRC8C, and LRRC8D on intracellular cGAMP signaling in TIME cells. Knockout pools were treated with 1 μM free or lipid-complexed cGAMP for 2 h and signaling was assessed by Western blot (n = 3 biological replicates).

(C) Effect of LRRC8A, LRRC8C, and LRRC8A/C on extracellular cGAMP signaling in TIME cells. Knockout pools were treated with 50 μM cGAMP for 2 h and signaling then assessed by Western blot (n = 3 biological replicates).

(D) Effect of LRRC8A, LRRC8A-R103L, or LRRC8C protein rescue on extracellular cGAMP signaling in TIME cells. Knockout cells were induced to express Flag-tagged protein constructs using doxycycline, then treated with 50 μM cGAMP for 2 h and signaling assessed by Western blot (n = 3 biological replicates).

(E) Cryo-EM structure of human homo-hexameric LRRC8A (PDB: 5ZSU) (Kasuya et al., 2018). Surface representation of the complex, with cartoon representation of two opposing LRRC8A subunits and zoom to the extracellular pore gating R103 residue.

For (A)–(D), representative blots are shown with quantification of all experiments displayed as mean ± SD. Significance calculated using ratio paired *t*-test; **P* ≤ 0.05, ***P* ≤ 0.01, ****P* ≤ 0.001, not significant (NS). See also Figure S4.

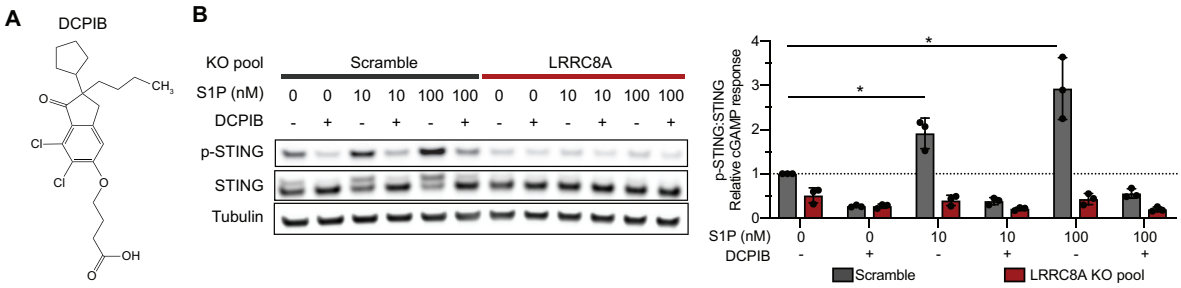

Figure 5. cGAMP Import by the LRRC8A:C Channel Can Be Potentiated by Sphingosine-1-Phosphate and Inhibited by DCPIB

(A) Chemical structure of DCPIB.

(B) Effect of sphingosine-1-phosphate (S1P) and DCPIB on extracellular cGAMP signaling in TIME cells. Scramble and LRRC8A knockout pools were treated with cGAMP (50 μM), with or without S1P (10 or 100 nM) and DCPIB (20 μM) for 1 h and signaling assessed by Western blot (n = 3 biological replicates). Representative blots are shown with quantification of all experiments displayed as mean ± SD. Significance calculated using ratio paired *t*-test; **P* ≤ 0.05. See also Figure S5.

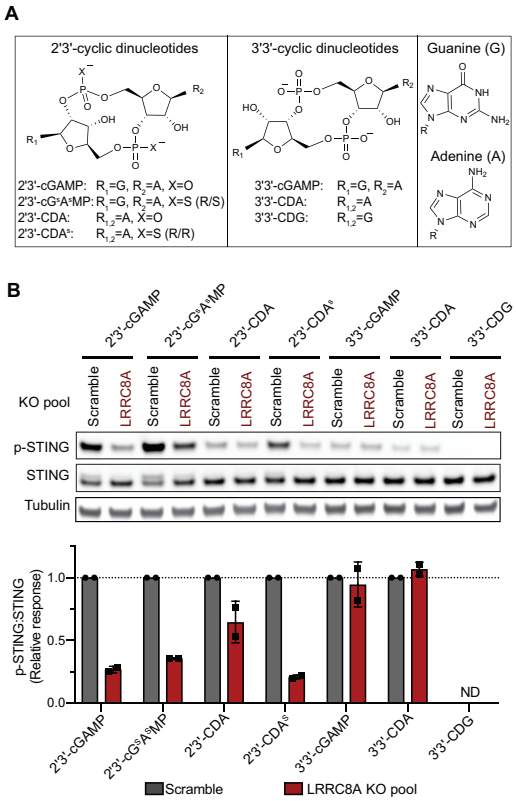

Figure 6. The LRRC8A:C Channel Imports Other 2'3'-Cyclic Dinucleotides

(A) Chemical structures of 2'3'- and 3'3'-cyclic dinucleotide (CDN) STING agonists.

(B) Importance of LRRC8A for signaling of various extracellular CDNs in TIME cells. Scramble and LRRC8A knockout pools were treated with 50 μM cGAMP, 25 μM 2'3'-cG^{S}A^{S}MP, 100 μM 2'3'-CDA, 25 μM 2'3'-CDA^S, 100 μM 3'3'-cGAMP, 200 μM 3'3'-CDA, or 200 μM 3'3'-CDG for 2 h and signaling assessed by Western blot (n = 2 biological replicates). Representative blots are shown with quantification of all experiments displayed as mean ± SD.

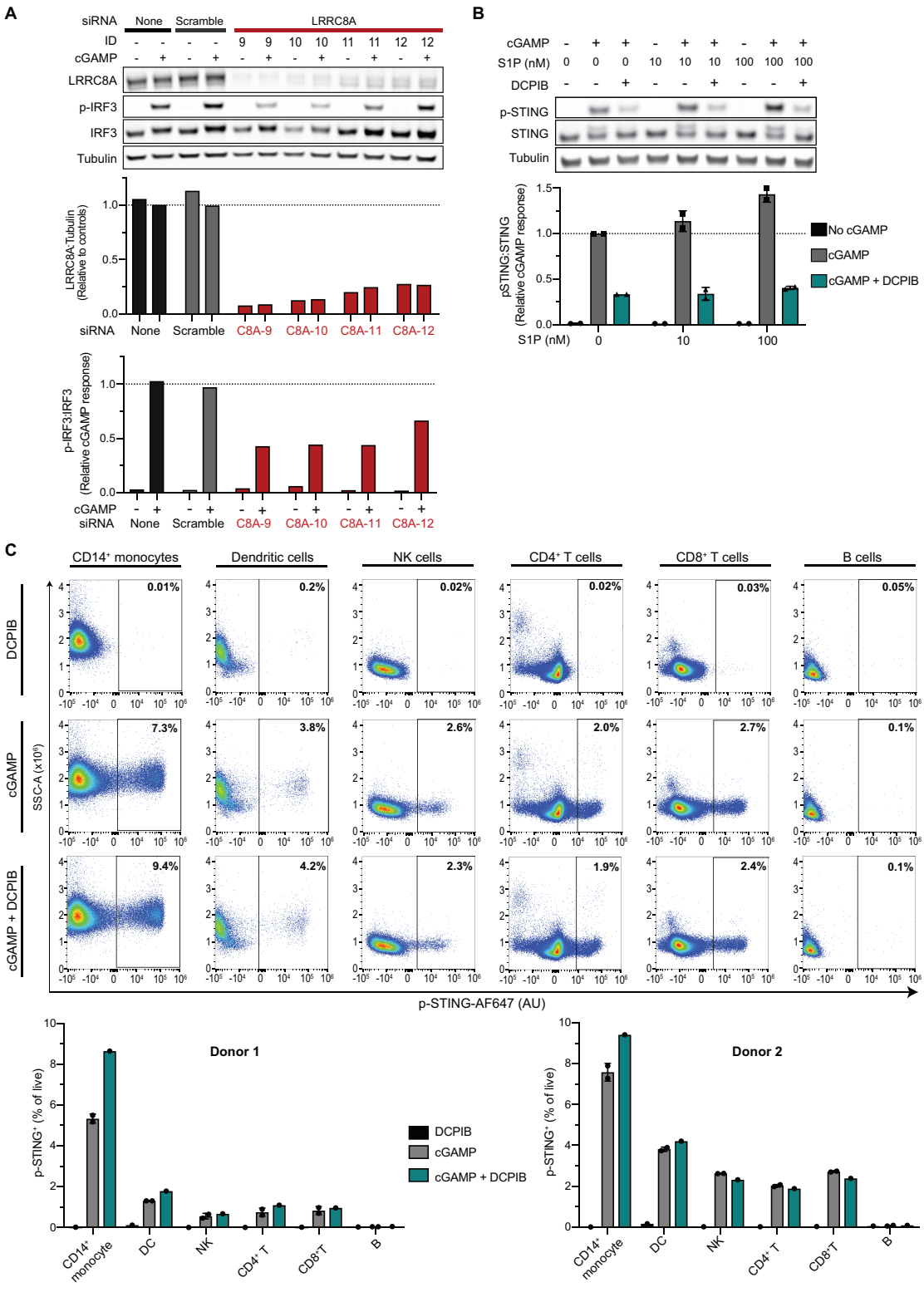

Figure 7. LRRC8A-Containing Channels Are the Dominant cGAMP Importer in Primary Human Endothelial Cells, but Not in PBMCs

(See next page for full figure legend)

Figure 7. LRRC8A-Containing Channels Are the Dominant cGAMP Importer in Primary Human Endothelial Cells, but Not in PBMCs

(A) Effect of LRRC8A on extracellular cGAMP signaling in primary HUVEC cells. Following siRNA knockdown of LRRC8A expression in HUVEC (4 d), cells were treated with cGAMP (100 μM) for 2 h. Western blots shown with quantification (n = 1).

(B) Effect of S1P and DCPIB on extracellular cGAMP signaling in HUVEC cells. Cells were treated with cGAMP (50 μM), with or without S1P (10 or 100 nM) and DCPIB (20 μM) for 1 h. Representative Western blots shown with quantification of mean ± SD (n = 2 biological replicates).

(C) Effect of extracellular cGAMP and DCPIB on PMBC cells. PBMCs isolated from two donors were treated with 100 μM cGAMP for 1.5 h with or without DCPIB and analyzed by flow cytometry (see Figure S7A for gating strategy). Representative plots are displayed with quantification across donors and subsets. For cGAMP treatment, results displayed as mean ± SD (n=2 technical replicates), remaining treatments (n=1). See also Figure S6.

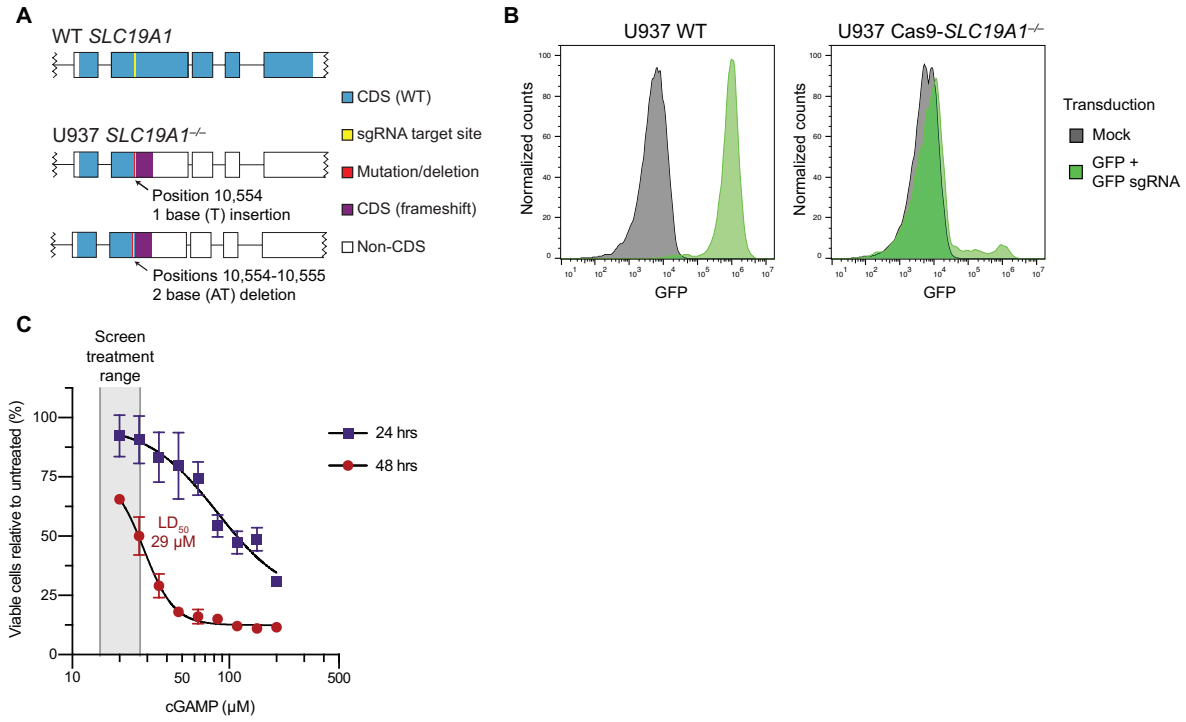

Figure S1. A Genome-Wide CRISPR Screen Identifies LRRC8A as a Positive Regulator of Extracellular cGAMP-Mediated STING Pathway Activation, Related to Figure 1

(A) Diagram of mutations in *SLC19A1* loci with predicted coding effects in the U937 Cas9-*SLC19A1*$^{-/-}$ line. Genomic DNA was isolated from cells and DNA flanking the *SLC19A1* sgRNA target site was sequenced. Editing is present in both alleles beginning at position 10,554 of the *SLC19A1* gene, with allele #1 containing an insertion and allele #2 containing a deletion. Both mutations result in a coding frameshift in exons 2 and 3, terminating in a premature stop in exon 3. Boxes represent coding exons of *SLC19A1* and horizontal lines represent introns.

(B) Plot of GFP expression measured as a test of Cas9 editing efficiency in the U937 Cas9-*SLC19A1*$^{-/-}$ line. U937 WT or U937 Cas9-*SLC19A1*$^{-/-}$ cells were untreated or transduced with lentivirus encoding GFP expression and GFP-targeting sgRNA. Transduced cells express GFP in the absence of Cas9, while Cas9 expression results in CRISPR knockout of GFP. Cells were analyzed for GFP expression by flow cytometry and data are displayed as histograms of ~10,000 events from each condition.

(C) Plot of percent live U937 *SLC19A1*$^{-/-}$ cells in response to cGAMP treatment after 24 or 48 h. Cells were counted by hemocytometry. Data are mean ± SD (n = 3 biological replicates at 24 h, n = 2 biological replicates at 48 h).

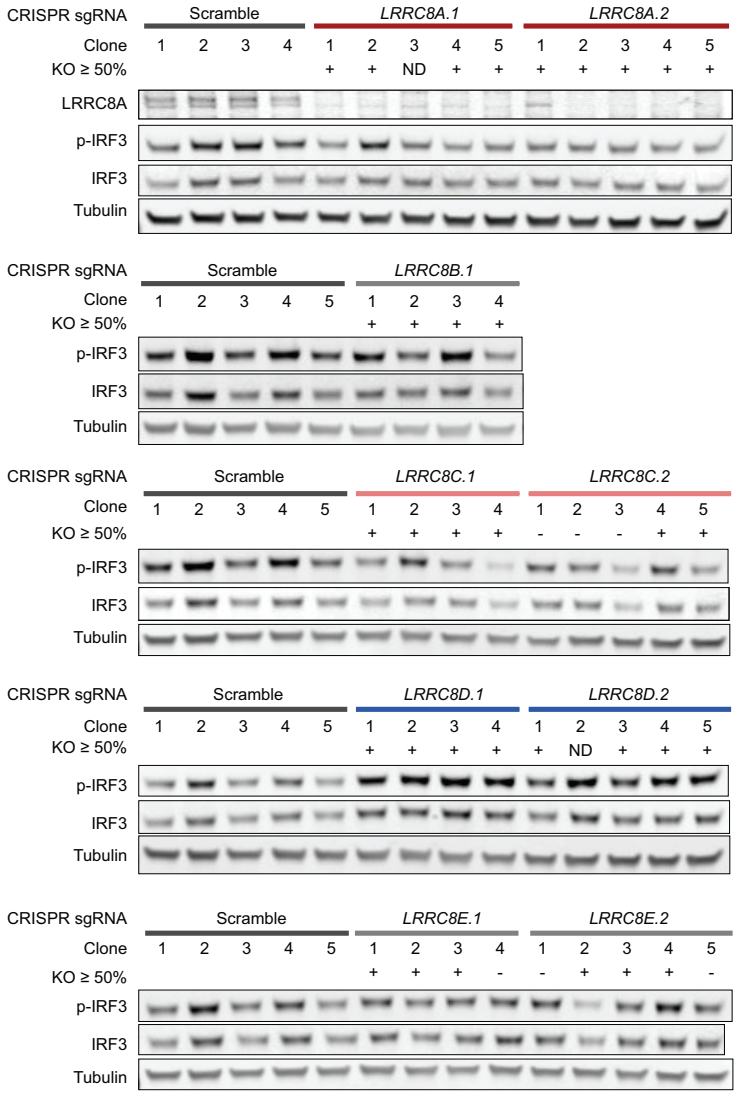

Figure S2. LRRC8A and LRRC8 Paralogs Differentially Facilitate cGAMP Import, Related to Figure 2

U937 *SLC19A1*$^{-/-}$ clones expressing scramble or *LRRC8A–E* sgRNAs were treated with 100 μM cGAMP for 4 h and signaling was measured by Western blot. Validation of CRISPR editing was confirmed by gDNA sequencing and Inference of CRISPR Edits (ICE) analysis. ICE knockout (KO) scores represent the proportion of sequences with a frameshift or >21 base pair insertion/deletion, with scores ≥ 50 found upon heterozygous or homozygous gene knockout. Not determined (ND) represents poor sequence traces preventing analysis. The same scramble clone lysates were run with each *LRRC8* knockout group, enabling the relative normalization of confirmed (KO ≥ 50) clones displayed in Figure 2A.

A

HEK293 CRISPR pool	ICE knockout score
sg*LRRC8A*.1	98
sg*LRRC8B*.1	83
sg*LRRC8C*.1	79
sg*LRRC8D*.2	88
sg*LRRC8E*.2	97

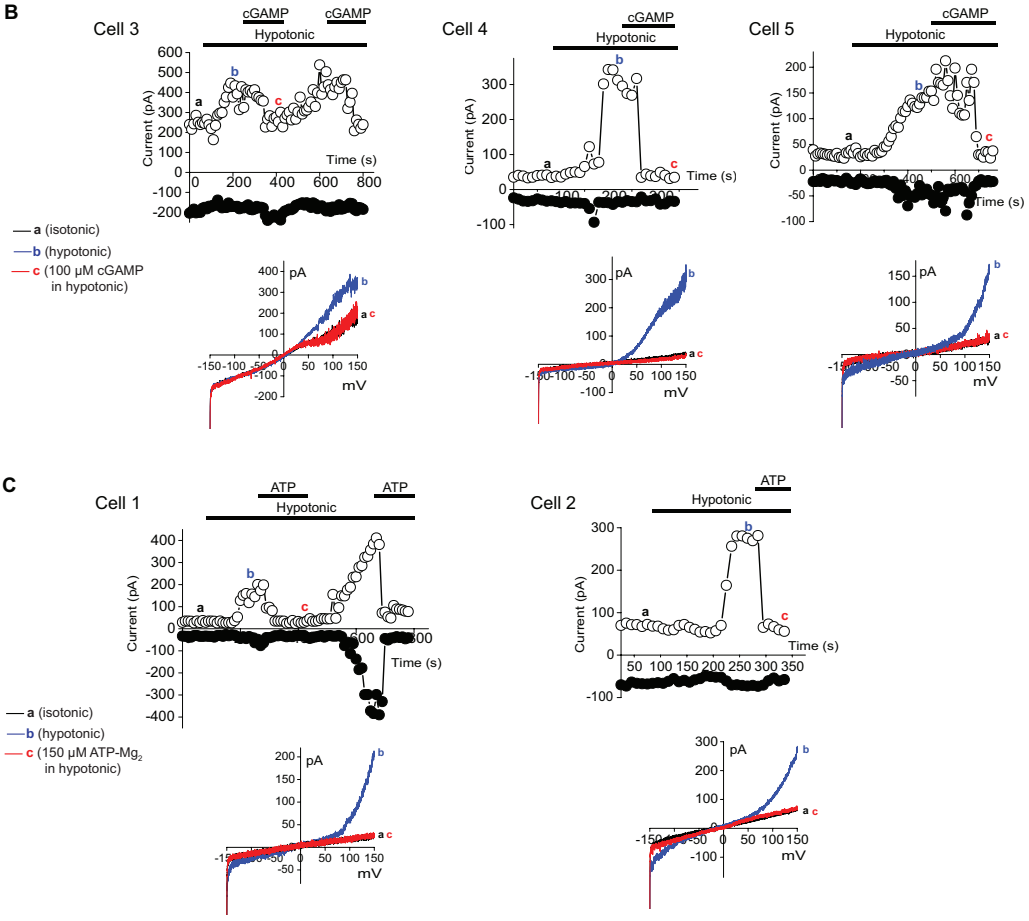

Figure S3. LRRC8A-Containing VRAC Channels Directly Transport cGAMP, Related to Figure 3

(A) Table reporting ICE knockout scores for HEK293 knockout pools, as determined from gDNA sequencing at the corresponding locus. Knockout scores represent the proportion of sequences with a frameshift or >21 base pair insertion/deletion.

(B) Representative whole-cell patch clamp current traces measured in HEK293 cells upon hypotonic stimulation in the absence or presence of cGAMP (100 μM). Overlays of the current-voltage relationship at the indicated points are also displayed. Traces for cells 1 and 2 are displayed in Figure 3C.

(C) Representative whole-cell patch clamp current traces measured in HEK293 cells upon hypotonic stimulation in the absence or presence of ATP (150 μM). Overlays of the current-voltage relationship at the indicated points are also displayed.

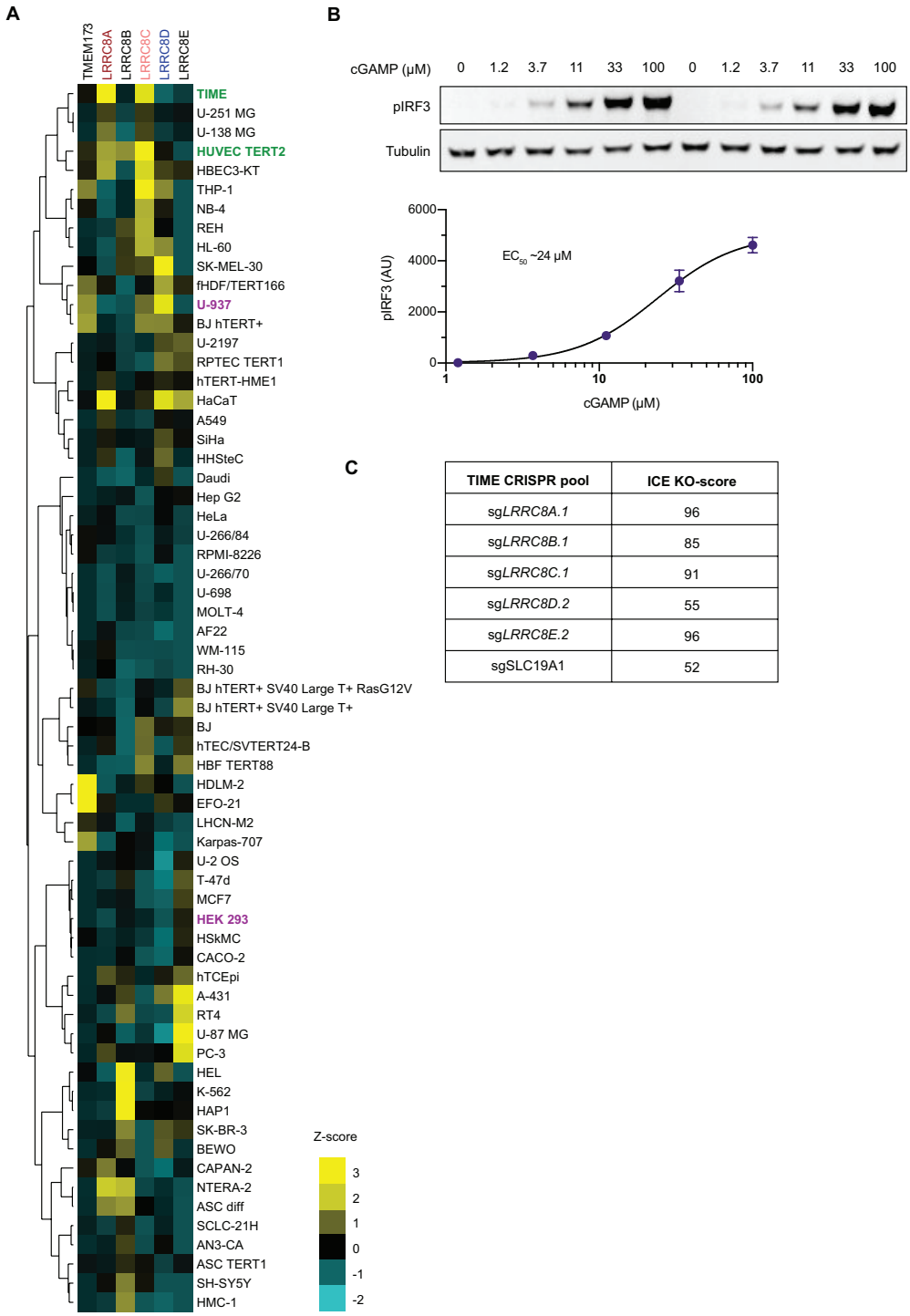

TIME CRISPR pool	ICE KO-score
sg*LRRC8A.1*	96
sg*LRRC8B.1*	85
sg*LRRC8C.1*	91
sg*LRRC8D.2*	55
sg*LRRC8E.2*	96
sgSLC19A1	52

Figure S4. The LRRC8A:C Channel Is the Dominant cGAMP Importer in Microvasculature Cells, Related to Figure 4

(See full legend on next page)

Figure S4. The LRRC8A:C Channel Is the Dominant cGAMP Importer in Microvasculature Cells, Related to Figure 4

(A) Heatmap of RNA transcript levels of *TMEM173* (STING) and *LRRC8* paralogs across common cell lines. Publicly available RNAseq data were downloaded from The Human Protein Atlas (proteinatlas.org). Minimum detectable expression was set to NX = 1 and Z-scores were then calculated within each transcript (observed $_{\text{transcript x}}$ – average $_{\text{transcript x}}$) / standard deviation $_{\text{transcript x}}$. Hierarchical clustering was applied for display of cells based on similarity of transcript profiles. Vasculature lineages are annotated in green text, and other lines studied in the paper are annotated in purple.

(B) Dose-response determination of extracellular cGAMP in TIME cells. Wild-type TIME cells were treated with cGAMP at the indicated concentrations for 2 h and signaling measured by Western blot. Data are mean ± SD (n = 2 technical replicates).

(C) Table reporting ICE knockout scores for TIME knockout pools, as determined from gDNA sequencing at the corresponding locus. The knockout score represents the proportion of sequences with a frameshift or >21 base pair insertion/deletion.

Figure S5. cGAMP Import by the LRRC8A:C Channel Can Be Potentiated by Sphingosine-1-Phosphate and Inhibited by DCPIB, Related to Figure 5

(A) TIME cells were treated with sphingosine-1-phosphate (S1P) with or without cGAMP for 1 h and STING pathway activation was assessed by Western blot (n = 1).

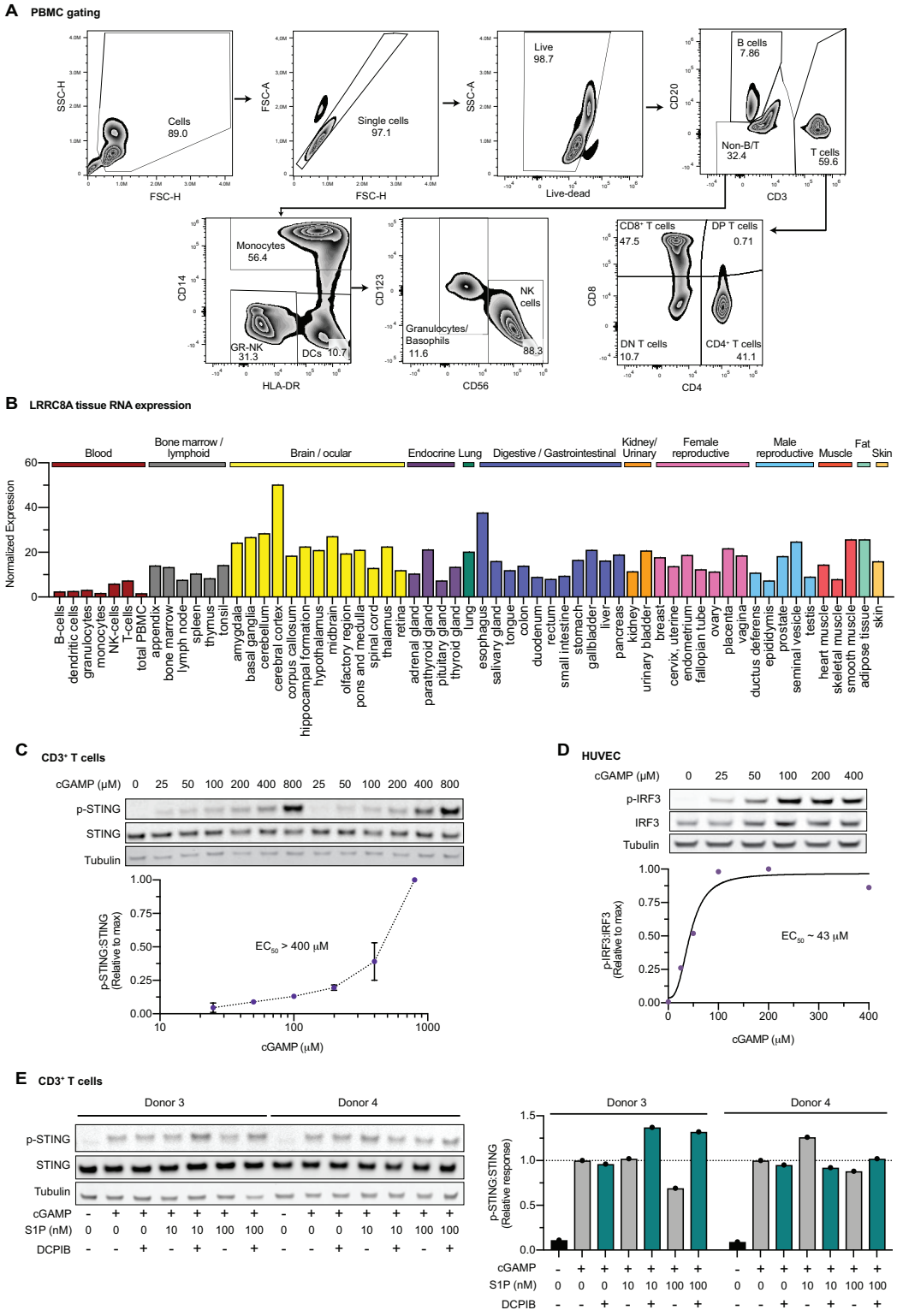

Figure S6. LRRC8A-Containing Channels Are the Dominant cGAMP Importer in Primary Human Endothelial Cells, but Not in PBMCs, Related to Figure 7

(See full legend on next page)

Figure S6. LRRC8A-Containing Channels Are the Dominant cGAMP Importer in Primary Human Endothelial Cells, but Not in PBMCs, Related to Figure 7

(A) Flow cytometry gating strategy used to identify cellular subsets in PBMCs.

(B) Plot of *LRRC8A* mRNA transcript levels across tissues. Publicly available data were downloaded from The Human Protein Atlas (proteinatlas.org).

(C) Dose-response determination for extracellular cGAMP in primary human $CD3^+$ T cells. Treatment with cGAMP was performed at the indicated concentrations for 2 h and signaling was measured by Western blot. Data are mean ± SD (n = 2 technical replicates).

(D) Dose-response determination for extracellular cGAMP in HUVEC cells. Treatment with cGAMP was performed at the indicated concentrations for 2 h and signaling was measured by Western blot (n = 1).

(E) Effect of S1P and DCPIB on cGAMP signaling in $CD3^+$ T cells. Isolated cells from two donors were treated with 100 μM cGAMP in the absence of presence of 10 or 100 nM S1P and 20 μM DCPIB for 1 h and signaling was measured by Western blot (two donors, n=1 per condition).

Experiment type	Antigen	Source	Clone [phospho site]	Dye conjugate	Manufacturer	Dilution factor
Western blot	p-STING	Rabbit	D7C3S [S366]	-	Cell Signaling Technology	1000
	p-TBK1	Rabbit	D52C2 [S172]	-		1000
	p-IRF3	Rabbit	4D4G [S396]	-		1000
	STING	Rabbit	D2P2F	-		1000
	TBK1	Rabbit	D1B4	-		1000
	IRF3	Rabbit	D83B9	-		1000
	α-tubulin	Mouse	DM1A	-		1000
	DYKDDDDK peptide ("FLAG")	Rabbit	Polyclonal	-		1000
	LRRC8A	Mouse	8H9	-	Sigma Aldrich	250
	LRRC8C	Rabbit	MBS711316	-	MyBioSource	500
	Rabbit IgG	Goat		800CW	LI-COR	10,000
	Mouse IgG (H+L)	Goat		680RD	LI-COR	10,000
Flow cytometry	p-STING	Rabbit	D8K6H, [Ser366]	AF647	Cell Signaling Technology	50
	CD14	Mouse	MΦP9	BUV395	BD	40
	HLA-DR	Mouse	G46-6	BUV661	BD	80
	CD56	Mouse	NCAM16.2	BUV737	BD	176
	CD20	Mouse	L27	BV450	BD	80
	CD4	Mouse	SK3	BV510	BD	80
	CD8	Mouse	RPA-T8	BV650	BD	40
	CD3	Mouse	UCHT1	AF488	BD	80
	CD123	Mouse	32703	AF700	R&D Systems	333

Table S1. Antibodies Used in This Study, Related to Experimental Methods.

Name	Sequence (5' to 3')
CRISPR screen NGS primers	
sgRNA_Fwd	aggcttggatttctataacttcgtatagcatacattatac
sgRNA_Rev	acatgcatggcggtaatacggttatc
LibraryPrep_Fwd	caagcagaagacggcatacgagatgcacaaaaggaaactcaccct
LibraryPrep_ID-1_Rev	aatgatacggcgaccaccgagatctacacGATCGGAAGAGCACACGTC TGAACTCCAGTCACCTTGTACGACTCGGTGCCACTTTTTC
LibraryPrep_ID-2_Rev	aatgatacggcgaccaccgagatctacacGATCGGAAGAGCACACGTC TGAACTCCAGTCACGCCAATCGACTCGGTGCCACTTTTTC
LibraryPrep_ID-3_Rev	aatgatacggcgaccaccgagatctacacGATCGGAAGAGCACACGTC TGAACTCCAGTCACAGTTCCCGACTCGGTGCCACTTTTTC
LibraryPrep_ID-4_Rev	aatgatacggcgaccaccgagatctacacGATCGGAAGAGCACACGTC TGAACTCCAGTCACTAGCTTCGACTCGGTGCCACTTTTTC
CRISPR sgRNA oligos	
sgLRRC8A.1	GGATCCTGAAGCCGTGGT
sgLRRC8A.2	GGCACCAGTACAACTACG
sgLRRC8B.1	GCCCAACTTCCAGTGTCC
sgLRRC8C.1	GTTATGAGCGAGCCCTCCAC
sgLRRC8C.2	GGAGATGAAATGTTCTATTT
sgLRRC8D.1	GATCTTTGGTAAGTTGCA
sgLRRC8D.2	GTTACCATCTGGCCCTTCCG
sgLRRC8E.1	GCTCATGATTGGGGTCTT
sgLRRC8E.2	GCTCCAGGAGAACTTATCAG
sgSLC19A1	GCACGAGAGAGAAGAATGT
Genomic DNA sequencing primers	
LRRC8A_gDNA_Fwd	TGGTCCTAGGAAAGCCAGGCC
LRRC8A_gDNA_Rev	AGTCGAAGCACTTCAGCAGG
LRRC8B_gDNA_Fwd	CAAGTCCAAGATTTTGCTTTCGTCC
LRRC8B_gDNA_Rev	GTCGATTTCAAGAGTGATGTGGG
LRRC8C_gDNA_Fwd	CCTGCTCAGAACCACTCTTCCC
LRRC8C_gDNA_Rev	AAAGACTGAGAGTTGACCAGGC
LRRC8D_gDNA_Fwd	CCTTGCGGAAGTTGCATCAC
LRRC8D_gDNA_Fwd	ACGCTTTTGTCGTCCAAGGG
LRRC8E_gDNA-1_Fwd	GAGGGTCTCTCTCTACACCCC
LRRC8E_gDNA-1_Rev	TAGCAATGTGGGGACTCCGG
LRRC8E_gDNA-2_Fwd	GGCCTCCCAAAGTGCTAGG
LRRC8E_gDNA-2_Rev	GGAGAGTCGAAACACTTGCCC
SLC19A1_gDNA_Fwd	TTCCTGCTCACCGACTACCTG
SLC19A1_gDNA_Rev	CCACCTCGTTCCACAGGATG

Table S2. Oligonucleotides Used in This Study, Related to Experimental Methods.